Mean curvature motion of point cloud varifolds

Blanche Buet, Martin Rumpf

ESAIM: M2AN 56 (2022) 1773–1808
https://doi.org/10.1051/m2an/2022047

ESAIM: Mathematical Modelling and Numerical Analysis
www.esaim-m2an.org

MEAN CURVATURE MOTION OF POINT CLOUD VARIFOLDS

Blanche Buet[1,*] and Martin Rumpf[2]

Abstract. This paper investigates a discretization scheme for mean curvature motion on point cloud varifolds with particular emphasis on singular evolutions. To define the varifold a local covariance analysis is applied to compute an approximate tangent plane for the points in the cloud. The core ingredient of the mean curvature motion model is the regularization of the first variation of the varifold *via* convolution with kernels with small stencil. Consistency with the evolution velocity for a smooth surface is proven provided that a sufficiently small stencil and a regular sampling are considered. Furthermore, an implicit and a semi-implicit time discretization are derived. The implicit scheme comes with discrete barrier properties known for the smooth, continuous evolution, whereas the semi-implicit still ensures in all our numerical experiments very good approximation properties while being easy to implement. It is shown that the proposed method is robust with respect to noise and recovers the evolution of smooth curves as well as the formation of singularities such as triple points in 2D or minimal cones in 3D.

Mathematics Subject Classification. 49Q20, 35K55, 53A70, 53E10.

Received March 15, 2021. Accepted May 6, 2022.

1. Introduction

In this paper we study the discretization of mean curvature motion for point cloud varifolds. Point clouds are the raw output data of 3D laser scanning devices and instead of applying a meshing algorithm which approximates the point cloud with a triangular surface we aim for geometry processing methods directly on the raw data. Particular emphasis is on a proper treatment of possibly noisy point distributions and geometric singularities such as triple points or crease lines.

The direct processing of point clouds has intensively been studied in the literature. Using the normal cycle from geometric measure theory Cohen-Steiner and Morvan [16] were able to robustly compute the shape operator of a triangular mesh and they gave explicit error bounds. Yang and Qian [38] used a moving least square approach to compute curvature quantities on point cloud surfaces. In Chazal *et al.* [13] investigated the curvature estimation problem in particular for point cloud data. They showed that different curvature measures can stably be computed for compact sets with positive μ-reach using distance functions to the set and evaluating curvatures on them. Mérigot *et al.* [31] used a covariance analysis based on the local Voronoi tesselation to compute a robust discrete curvature for a point cloud surface. Yang *et al.* [39] used barycenters of spherical neighborhoods on

Keywords and phrases. Point cloud varifolds, Mean curvature motion, Regularization, Singular evolution, Time discretization.

[1] Université Paris-Saclay, INRIA, CNRS, Laboratoire de mathématiques d'Orsay, 91405 Orsay, France.
[2] Institute for Numerical Simulation, University of Bonn, Endenicher Allee 60, 53115 Bonn, Germany.
*Corresponding author: blanche.buet@u-psud.fr

multiple scales to derive formulas for the principle curvatures of a surface. This approach is based on the observation that the vector offset between barycenters for different radii of the balls or spheres depends on the surface curvature. Chazal *et al.* [13] followed the same approach and showed how this can be used to obtain approximations of generalized notions of curvature proposed by Federer.

In the processing of discrete surfaces the evolution by mean curvature motion is a fundamental tool and one of the basic fairing algorithms [18]. For the numerical discretization of mean curvature motion for hypersurfaces there are three widespread approaches corresponding to the representation of the hypersurfaces as a triangular surface [3, 17, 19], a level set [21, 30, 36], or a diffusive phase field interface [9, 23, 24]. For the representation of surfaces by point clouds a mean curvature motion scheme has been derived in [15] based on the reconstruction of a local triangulation. In [34] a special type of surface covering is defined for point clouds, which enable the stable evaluation of surface Laplacians and associated evolution problems.

The varifold perspective has been used in the context of curve or surface matching in [27] based on earlier work in [11]. Here, a set of simplices and simplex normals is encoded as a measure on $\mathbb{R}^n \times S^{n-1}$ and equipped with the structure of a reproducing kernel Hilbert space with suitable kernels for the position in $\mathbb{R}^n$ and the orientation in S^{n-1}. This approach is then used for the registration of curves and surfaces without point to point correspondence. A recent overview of these tools in the context of diffeomorphic registration can be found in [12].

In the context of this paper, we adopt a varifold perspective on point clouds and take advantage of the framework developed in [10] to estimate mean curvature with theoretical convergence guarantees. More precisely, we define a point cloud varifold by applying a local covariance analysis on the input set of points. This allows us to assign an approximate tangent space as well as a weight to each point. This leads to a natural varifold structure where point clouds are encoded through a weighted sum of Dirac masses plus orientation. We can subsequently consider the first variation of such a varifold and apply a suitable regularization *via* the convolution with a kernel with small stencil. The resulting regularized first variation is considered as the motion field for the mean curvature flow and an implicit and a semi-implicit time discretization are derived.

A particularity when processing directly point clouds is that it allows topological changes, concentration and merging of points very naturally. As consequence, while the formation of a triple point is a singularity at the continuous level, it is not from the point of view of point cloud evolution. We take advantage of this feature to recover some well–known minimizing sets like Steiner trees connecting the vertices of a square in 2D and minimal cones over the edges of a tetrahedron, which is known to be one of the basic minimal cones in 3D together with the plane and the triple junction of half-planes [37]. Furthermore, we compute minimal area sets spanned by the edges of a cube. However, while we can compare the limit set for time tending to infinity with sets that are known to be minimal (or at least with competitors with respect to surface area measures), the theoretical context for the evolution is not clear.

As we are dealing with a mean curvature discretization derived thanks to varifolds tools, it is very natural to think of Brakke flow that generalizes the notion of mean curvature flow to varifolds (see the seminal paper of Brakke [6] and the existence theorem of Brakke flow moving with singularities established by Kim and Tonegawa in [28]). Nevertheless, Brakke's construction evolves the whole varifold structure, pushing the positions by the mean curvature vector H and updating the tangent planes using the differential of H. On the other hand, the discrete flow under study only evolves positions of the points while tangents are updated from the positions, which is actually an important difference. Furthermore, we do not propagate density along the flow but we rather compute a weight for each point, again from the positions, in order to enforce a multiplicity 1 everywhere. Assuming a unit multiplicity is reasonable when starting from a compact hypersurface, indeed, it has been proven in [22] that for almost all neighboring level sets, there exists a unique Brakke flow, with unit multiplicity for almost all times.

We stress that results on existence and uniqueness beyond the creation of singularities are mostly obtained under the assumption that the set evolving by mean curvature can be represented as the boundary of some open set (which is in general not the case for Brakke flow). We mention two major approaches: in [14, 21] the issue is tackled through so-called viscosity solutions while [25] is based on the Allen-Cahn phase field model. In the case

of planar networks, the flow has been studied in [29] starting from a regular network, that is restricted to triple point singularities, and more recently the case of more general junctions could be handled in [26]. Note that in our simulations, we observe that four junctions in the initial data instantaneously split into two triple junctions, consistently with what is expected for planar networks. On the numerical side, all parametric (mesh based) approaches work with a fixed topology and enable under this constraint very good approximation results, *e.g.* in [8,32,33] with the drawback that there is an *a priori* choice or a required combinatorial optimization among all possible layouts of the smooth patches.

We emphasize two main contributions of this paper. First, we propose a numerical scheme that performs mean curvature motion beyond the creation of singularities. Taking advantage of the flexibility of point cloud representation, there is no *a priori* choice on the structure of singularities and expected minimal cones naturally form as smooth portions collapse. We illustrate the strength of this approach in Figures 7–11 where we are able to recover well-known singular soap films. Besides those conclusive numerical experiments, such a flow satisfies discrete counterparts to comparison principles that hold for mean curvature flow as described in Section 5.3. We also provide with Theorem 4.8 an improved convergence result for the approximate mean curvature. The assumptions on the limit varifold are weak enough (recalling that we are dealing with curvature issues): we require that the first variation is Radon and the mass of the varifold is Ahlfors regular. Introducing a divergence (4.5) among varifolds, based on flat and Prokhorov type distances, we are able to prove the convergence under the minimal assumption of weak star convergence of varifolds, with a quantitative and spatially uniform speed. Former results stated in [10] required, in turn, technical assumption (5.24) adding up to weak star convergence. We point out that proving a convergence result on curvature assuming only weak star convergence of discrete objects allows to embrace a wide class of discretizations.

The paper is organized as follows. In Section 2 we recall classical facts concerning varifolds, focusing on the so-called first variation and generalized mean curvature. Using a regularization *via* convolution, we define in Section 3 the generalized mean curvature model for point clouds varifolds and establish its consistency in Proposition 3.3. Its stability is then investigated in Section 4, resulting in Theorem 4.8 and convergence stated in Corollary 4.9. Section 5 describes how we define a point cloud varifold from a set of points *i.e.* how we compute tangent planes and weights for each point. Furthermore, we define time continuous curvature motion of point clouds, study planar and spherical comparison principles, and derive implicit and semi-implicit time discretization schemes. Finally in Section 6 we present numerical results and discuss properties of the derived scheme.

2. Varifolds and generalized mean curvature

In this section we will review the basic notions of d-varifolds in $\mathbb{R}^n$ and first variation of such varifolds. Of particular interest for this paper will be the case of generalized curves in $\mathbb{R}^2$ ($d = 1$, $n = 2$) and generalized surfaces in $\mathbb{R}^3$ ($d = 2$, $n = 3$). The d–dimensional Hausdorff measure in $\mathbb{R}^n$ is denoted by $\mathcal{H}^d$, and the space of continuous compactly supported function between two metric spaces by $\mathrm{C}_c(X, Y)$ and $\mathrm{C}_c(X)$ if $Y = \mathbb{R}$. The d–Grassmannian

$$G_{d,n} = \{d\text{–vector subspace of } \mathbb{R}^n\}.$$

is embedded into $n \times n$ matrices *via* the mapping that associates with the d–subspace $P \in G_{d,n}$ the orthogonal projector Π_P onto P. The operator norm on matrices consequently induces a distance on $G_{d,n}$. With this notation at hand let us give the definition of a d-varifold.

Definition 2.1 (Varifold)**.** A d–varifold in an open set $\Omega \subset \mathbb{R}^n$ is a Radon measure in $\Omega \times G_{d,n}$.

For detailed discussions on varifolds and underlying geometric measure theory tools we refer to [1,35]. We thereafter consider d–varifolds in the whole space $\Omega = \mathbb{R}^n$. Such measures can be understood as a coupling of spatial (in $\mathbb{R}^n$) and directional (in $G_{d,n}$) information. Integrating on all possible directions, that is on the whole Grassmannian, allows to select the spatial information encoded in a d–varifold V: the resulting Radon measure

denoted by $\|V\|$ is called the *mass* of V and is defined in $\mathbb{R}^n$ as

$$\|V\|(A) = V(A \times G_{d,n}).$$

for all Borel sets $A \subset \mathbb{R}^n$.

In this paper, we will focus on two types of varifolds: varifolds associated with a smooth d–submanifold of $\mathbb{R}^n$ (referred to as *smooth varifolds*, see Def. 2.2) and varifolds associated with a finite set of points in $\mathbb{R}^n$, positive weights and tangent d–planes in $G_{d,n}$ (referred to as *point cloud varifolds*, see Def. 2.4).

Definition 2.2 (Smooth varifold)**.** The d–varifold V associated with a d–submanifold $M \subset \mathbb{R}^n$ is defined by

$$V(B) = \mathcal{H}^d\left(\{x \in M : (x, T_x M) \in B\}\right), \tag{2.1}$$

for every Borel set $B \subset \mathbb{R}^n \times G_{d,n}$. Here, $T_x M$ denotes the tangent plane at x. In this case, $\|V\| = \mathcal{H}^d_{|M}$. We will use the notation $V = \mathcal{H}^d_{|M} \otimes \delta_{T_x M}$ for the varifold defined in (2.1).

Smooth varifolds are a particular case of *rectifiable varifolds* (see [35]).

Remark 2.3. As a d-varifold is a Radon measure, it can be equivalently defined by its action on continuous compactly supported functions: V is the smooth varifold associated with M according to Definition 2.2 if and only if for every $\varphi \in \mathrm{C}_c(\mathbb{R}^n \times G_{d,n})$,

$$\begin{aligned}\int_{(x,S)\in\mathbb{R}^n\times G_{d,n}} \varphi(x,S)\, dV(x,S) &= \int_{x\in\mathbb{R}^n\cap M} \int_{S\in G_{d,n}} \varphi(x,S) d\delta_{T_x M}(S)\, d\mathcal{H}^d(x) \\ &= \int_M \varphi(x, T_x M)\, d\mathcal{H}^d(x).\end{aligned}$$

Definition 2.4 (Point cloud varifold)**.** Given a finite set of points $\{x_i\}_{i=1}^N \subset \mathbb{R}^n$, masses (weights) $\{m_i\}_{i=1}^N \subset \mathbb{R}_+^*$ and space of directions $\{P_i\}_{i=1}^N \subset G_{d,n}$, we associate the d–varifold

$$V = \sum_{i=1}^N m_i \delta_{(x_i,P_i)} \quad \text{and in this case} \quad \|V\| = \sum_{i=1}^N m_i \delta_{x_i}.$$

Note that P_i can be any set of directions in $G_{d,n}$, however if the points $\{x_i\}_i$ sample some surface or submanifold M, then $\{P_i\}_i$ can be thought of as tangent planes $T_{x_i} M$.

As in the case of smooth varifolds, we can define a point cloud varifold through its action on compactly supported continuous functions. Indeed, we have for $\varphi \in \mathrm{C}_c(\mathbb{R}^n \times G_{d,n})$

$$\int \varphi\, dV = \sum_{i=1}^N m_i \varphi(x_i, P_i).$$

The set of d–varifolds is endowed with a weak notion of mean curvature which we eventually define in Definition 2.7. At first, let us introduce the *first variation*, which is well–defined for any d–varifold. For this purpose we need the following differential operators: let $P \in G_{d,n}$, Π_P be the orthogonal projection onto P and $(\tau_1, \dots, \tau_d)$ be an orthonormal basis of P, let $X = (X_1, \dots, X_n) \in \mathrm{C}^1(\mathbb{R}^n, \mathbb{R}^n)$ be a vector field of class C^1, $\varphi \in \mathrm{C}^1(\mathbb{R}^n)$ and $(e_1, \dots, e_n)$ be the canonical basis of $\mathbb{R}^n$, then

$$\nabla^P \varphi = \Pi_P(\nabla \varphi) \quad \text{and} \quad \mathrm{div}_P X = \sum_{i=1}^n \Pi_P(\nabla X_i) \cdot e_i = \sum_{i=1}^d DX\tau_i \cdot \tau_i.$$

Now, with these differential operators at hand we can define the first variation:

Definition 2.5 (First variation of a varifold, [2])**.** The first variation of a d–varifold V in $\mathbb{R}^n$ is the *distribution of order* 1

$$\begin{aligned}\delta V : \mathrm{C}^1_c(\mathbb{R}^n,\mathbb{R}^n) &\to \mathbb{R}\\ X &\mapsto \int_{\mathbb{R}^n\times G_{d,n}} \mathrm{div}_S X(x)\, dV(x,S).\end{aligned}$$

Remark 2.6. We could equivalently define the first variation based on scalar test functions. Indeed, with a slight misuse of notation define for $\varphi \in \mathrm{C}^1_c(\mathbb{R}^n)$,

$$\delta V(\varphi) := (\delta V(\varphi e_1),\dots,\delta V(\varphi e_n)) = \sum_{i=1}^n \delta V(\varphi e_i) e_i \quad \text{so that} \quad \delta V(X) = \sum_{i=1}^n \delta V(X\cdot e_i)\cdot e_i.$$

Moreover, $\mathrm{div}_S(\varphi e_i) = \nabla^S\varphi \cdot e_i$ and finally $\delta V(\varphi) = \int_{\mathbb{R}^n\times G_{d,n}} \nabla^S\varphi(x)\, dV(x,S)$.

Let $M \subset \mathbb{R}^n$ be a closed C^2 d–submanifold, if $V = \mathcal{H}^d_{|M} \otimes \delta_{T_xM}$ is the smooth varifold naturally associated with M, then by definition of V (see Rem. 2.3),

$$\int_{\mathbb{R}^n\times G_{d,n}} \mathrm{div}_S X(x)\, dV(x,S) = \int_M \mathrm{div}_{T_xM} X(x)\, d\mathcal{H}^d(x),$$

and thus, thanks to the divergence theorem we obtain for every $X \in \mathrm{C}^1_c(\mathbb{R}^n,\mathbb{R}^n)$,

$$\delta V(X) = \int_M \mathrm{div}_{T_xM} X(x)\, d\mathcal{H}^d(x) = -\int_M H(x)\cdot X(x)\, d\mathcal{H}^d(x),$$

where H is the mean curvature vector of M. In this case δV is more regular than a distribution of order 1, it is a distribution of order 0 and can be identified thanks to Riesz theorem with the vector valued Radon measure

$$-H(x)\,\mathcal{H}^d_{|M}(x) = -H(x)\,\|V\|(x). \tag{2.2}$$

Actually, as soon as V is a d–varifold (not necessarily associated with a smooth submanifold) whose first variation is a distribution of order 0 (V is then said to have *locally bounded first variation*), then there is a weak counter-part to the divergence theorem. Indeed, for such a varifold, we can identify the distribution δV with the associated Radon measure provided by Riesz theorem. Then, thanks to the Radon-Nikodym decomposition of δV with respect to the mass $\|V\|$, there exist a vector field denoted $\frac{\delta V}{\|V\|} \in \mathrm{L}^1_{loc}(\|V\|)$ and a Radon measure $(\delta V)_s$ singular with respect to $\|V\|$ (which might vanish) such that the decomposition

$$\delta V = \frac{\delta V}{\|V\|}(x)\,\|V\| + (\delta V)_s \tag{2.3}$$

holds. Comparing (2.2) and (2.3) the *generalized mean curvature vector* naturally arises as the Radon-Nikodym derivative $H = -\dfrac{\delta V}{\|V\|}$. Let us resume the previous observations in the following definition.

Definition 2.7 (Generalized mean curvature, [2])**.** Let V be a d–varifold in $\mathbb{R}^n$. Assume that V has *locally bounded first variation*, *i.e.* $\forall K \subset \mathbb{R}^n$ compact set, $\exists c_K > 0$ such that for every $X \in \mathrm{C}^1_c(\mathbb{R}^n,\mathbb{R}^n)$ supported in K,

$$|\delta V(X)| \le c_K \sup_K |X|. \tag{2.4}$$

Then δV can be identified with a Radon measure and the *generalized mean curvature vector* H is defined as the Radon-Nikodym derivative of δV with respect to $\|V\|$, moreover, for $\|V\|$–a.e. x and for $B(x,r)$ denoting the open ball of radius r centered at x we get

$$H(x) = -\lim_{r\to 0_+} \frac{\delta V(B(x,r))}{\|V\|(B(x,r))}.$$

See Section 2.4 in [1] for more details on differentiation of Radon measures. Notice that both classical and the generalized mean curvature coincide in the case of a smooth varifold associated with a closed C^2 manifold as shown above (2.2).

Let us now consider an example involving a triple point singularity.

Example 2.8 (Junction of half-lines)**.** Let u_1, u_2, u_3 be unit vectors of $\mathbb{R}^2$ and D_i for $i \in \{1,2,3\}$ be the half-line $\{tu_i \,:\, t \in \mathbb{R}_+\}$ and $V_i = \mathcal{H}^1_{|D_i} \otimes \delta_{\mathrm{span(u_i)}}$ be the smooth 1–varifold associated with D_i. Then $V = V_1 + V_2 + V_3$ is a 1–varifold spatially supported by the union of three half-lines meeting at 0 and by linearity $\delta V = \delta V_1 + \delta V_2 + \delta V_3$. Now, we obtain $\delta V_i = -u_i \delta_0$ for $i \in \{1,2,3\}$. Indeed, for $X \in \mathrm{C}^1_c(\mathbb{R}^2, \mathbb{R}^2)$ and for $t \in \mathbb{R}_+$, $\mathrm{div}_{\mathrm{span(u_i)}} X(tu_i) = DX(tu_i)u_i \cdot u_i$ and $DX(tu_i)u_i = \dfrac{d}{dt}(X(tu_i))$, therefore:

$$\delta V_i(X) = \int_{D_i} \mathrm{div}_{\mathrm{span(u_i)}} X \, d\mathcal{H}^1 = \int_{t=0}^{+\infty} \frac{d}{dt}(X(tu_i))\, dt \cdot u_i = -X(0) \cdot u_i = -\delta_0(X) \cdot u_i.$$

We eventually obtain $\delta V = -(u_1 + u_2 + u_3)\delta_0$ and in particular $\delta V = 0$ if and only if 0 is a triple point with angles $\frac{2}{3}\pi$ formed by the half-lines. Otherwise, if $u_1 + u_2 + u_3 \neq 0$, the singularity in 0 produces a non-zero singular curvature $(\delta V)_s = -(u_1 + u_2 + u_3)\delta_0$.

We emphasize that the notion of first variation is well–defined for any d–varifold while the notion of generalized mean curvature requires some additional regularity of the varifold: it can be defined only if V has locally bounded first variation in the sense of (2.4) that is equivalent to requiring that δV identifies with a (vector–valued) Radon measure thanks to Riesz representation theorem. In the previous example, though singular with respect to the mass measure $\|V\| = \mathcal{H}^1_{|D_1} + \mathcal{H}^1_{|D_2} + \mathcal{H}^1_{|D_3}$, the first variation $\delta V = -(u_1 + u_2 + u_3)\delta_0$ is a Dirac mass that is, in particular, a Radon measure. Unfortunately, the first variation of a point cloud varifold does not meet this assumption, as we now explain. Let us consider a very simple point cloud 1–varifold in $\mathbb{R}$ consisting of one single point $x_1 = 0$ weighted by mass $m_1 = 1$ and with $P_1 = \mathbb{R}$: $V = \delta_{(0,\mathbb{R})}$. For $X \in \mathrm{C}^1_c(\mathbb{R}, \mathbb{R})$ we obtain in this case

$$\delta V(X) = \int_{\mathbb{R}} \mathrm{div}_{\mathbb{R}} X \, d\delta_0 = \mathrm{div}_{\mathbb{R}} X(0) = X'(0) = \delta_0(X') = -(\delta_0)'(X).$$

It is well–known that the distributional derivative of a Dirac mass is not a Radon measure. In fact, this observation directly extends to any point cloud varifold $V = \sum_{i=1}^N m_i \delta_{(x_i,P_i)}$ and the first variation of V is never locally bounded (take test functions whose support contains a single point x_i). This was the motivation for introducing in [10] approximate counterparts of first variation and generalized mean curvature *via* convolution. In this paper we will make extensive use of these notions. We hence summarize in the next section what is needed within the scope of this paper.

3. Regularization *via* convolution

In the first part of this section we recall a regularization of the generalized mean curvature (see Def. 3.2) based on the convolution of both first variation and mass with appropriately chosen kernels. The original definition of this regularized mean curvature from [10] ensures consistency for a very large class of varifolds (rectifiable varifolds with locally bounded first variation). In the second part of the section, we will introduce several variants of a regularized mean curvature vector which are all consistent with the mean curvature vector of a smooth hypersurface (see Prop. 3.3). The difference lays in the choice of a projection operator denoted by Π hereafter. As we will see in Sections 5.3 and 6 the concrete choice of the projection operator Π matters on one hand in the presence of singularities and on the other hand for the numerical stability of the time discrete scheme.

From now on and for the sake of simplicity, we only consider varifolds with finite mass, that is $\|V\|(\mathbb{R}^n) < \infty$ (as $\|V\|$ is a Radon measure, $\|V\|$ is finite when restricted to any bounded open set). We refer to [10] for additional details on steps leading to the notion of approximate mean curvature (see Def. 3.2) that we now briefly sketch.

Let us consider fixed functions $\rho, \xi \in \mathrm{C}^\infty(\mathbb{R})$, which are nonnegative even and compactly supported in $[-1,1]$. We additionally assume that ρ and ξ are positive in $]0,1[$ and ρ is nonincreasing in $[0,1]$.

Then we define associated mollifiers $(\rho_\varepsilon)_{\varepsilon>0}$, $(\xi_\varepsilon)_{\varepsilon>0}$ in $\mathbb{R}^n$ as follows: for $x \in \mathbb{R}^n$, $\varepsilon > 0$, $\rho_\varepsilon(x) = \varepsilon^{-n}\rho(|x|/\varepsilon)$ and $\xi_\varepsilon(x) = \varepsilon^{-n}\xi(|x|/\varepsilon)$. We additionally assume that for all $s \in]-1,1[$,

$$n\xi(s) = -s\rho'(s), \tag{3.1}$$

that is, we can fix ρ and then define ξ satisfying the above equation. Note that such a choice (*e.g.* compared with $\xi = \rho$) improves numerical stability of the approximate mean curvature, as already detailed in Section 6 of [10]. Interestingly, (3.1) appears to be a crucial point when stating comparison principle in Sections 5 and 5.3, see for instance proof of Proposition 5.2.

For instance we can choose

$$\rho(s) = \exp\left(\frac{1}{s^2-1}\right) \quad \text{and} \quad \xi(s) = \frac{2}{n}\frac{s^2}{(s^2-1)^2}\exp\left(\frac{1}{s^2-1}\right) \quad \text{for } s \in]-1,1[.$$

The *ε–regularized first variation* is then defined as the convolution of δV with ρ_ε: for $X \in \mathrm{C}^1_c(\mathbb{R}^n, \mathbb{R}^n)$,

$$(\delta V * \rho_\varepsilon)(X) := \delta V(X * \rho_\varepsilon) \quad \text{with} \quad (X * \rho_\varepsilon)(x) := \int_{y\in\mathbb{R}^n} \rho_\varepsilon(x-y)X(y)dy.$$

Easy computations lead to $(\delta V * \rho_\varepsilon)(X) = \displaystyle\int_{\mathbb{R}^n} g_\varepsilon(x)\cdot X(x)\,dx$, where

$$g_\varepsilon(x) = \frac{1}{\varepsilon^{n+1}}\int_{\mathbb{R}^n\times G_{d,n}} \rho'\left(\frac{|y-x|}{\varepsilon}\right)\Pi_S\left(\frac{y-x}{|y-x|}\right)dV(y,S) =: \delta V * \rho_\varepsilon(x) \quad \text{for } x \in \mathbb{R}^n. \tag{3.2}$$

Consequently $\delta V * \rho_\varepsilon$ identifies with its Lebesgue L^1–density $g_\varepsilon \in \mathrm{L}^1_{loc}(\mathbb{R}^n)$.

Remark 3.1. Note that $\rho'(|z|)\frac{z}{|z|} \xrightarrow[|z|\to 0]{} 0$ thanks to $\rho'(0) = 0$.

In order to define a regularized generalized mean curvature, it remains to write the Radon-Nikodym decomposition of the regularized first variation $\delta V * \rho_\varepsilon$ with respect to the regularized mass $\|V\| * \xi_\varepsilon$. As for the first variation, we identify $\|V\| * \xi_\varepsilon$ with the associated Lebesgue L^1–density function defined as

$$\|V\| * \xi_\varepsilon(x) = \frac{1}{\varepsilon^n}\int_{\mathbb{R}^n} \xi\left(\frac{|y-x|}{\varepsilon}\right)d\|V\|(y), \quad x \in \mathbb{R}^n.$$

Considered as Radon measures, both $\delta V * \rho_\varepsilon$ and $\|V\| * \xi_\varepsilon$ are absolutely continuous with respect to Lebesgue measure and consequently the Radon-Nikodym decomposition of $\delta V * \rho_\varepsilon$ with respect to $\|V\| * \xi_\varepsilon$ is

$$\delta V * \rho_\varepsilon = \frac{\delta V * \rho_\varepsilon(x)}{\|V\| * \xi_\varepsilon(x)}(\|V\| * \xi_\varepsilon) = \underbrace{\frac{\delta V * \rho_\varepsilon(x)}{\|V\| * \rho_\varepsilon(x)}}_{\to \frac{\delta V}{\|V\|}} \underbrace{\frac{\|V\| * \rho_\varepsilon(x)}{\|V\| * \xi_\varepsilon(x)}}_{\to \frac{\int_0^1 \rho(s)s^{d-1}ds}{\int_0^1 \xi(s)s^{d-1}ds} = \frac{n}{d}} (\|V\| * \xi_\varepsilon)$$

Finally, we obtain the following definition for the approximate mean curvature

Definition 3.2 (Approximate mean curvature ([10], 4.1))**.** Let V be a d–varifold in $\mathbb{R}^n$, for $x \in \mathbb{R}^n$, $\varepsilon > 0$, we define

$$H_\varepsilon(x,V) := -\frac{d}{n}\frac{\delta V * \rho_\varepsilon(x)}{\|V\| * \xi_\varepsilon(x)} \tag{3.3}$$

which we refer to as *ε–approximate curvature.*

The ratio $\frac{d}{n}$ is due to the particular choice of ξ and ρ fulfilling (3.1). Note that we could take other kernel functions not necessarily satisfying relation (3.1)) to regularize the first variation δV and the mass $\|V\|$ (*e.g.* the same kernel both for the variation and the mass). In this case the consistency when $\varepsilon \to 0$ would still hold replacing d/n in (3.3) by the appropriate constant. Nevertheless, (3.1) gives better numerical results that can be understood by expanding $|H(x) - H_\varepsilon(x, V)|$ when $\varepsilon \to 0$ (see [10]). We point out that this very same assumption (3.1) on the kernels enables us to prove a discrete maximum principle on our time discrete scheme (see Prop. 5.4).

Finally, let us remark that no assumption on δV is necessary to define $H_\varepsilon(\cdot, V)$. It is well–defined even if δV is not locally bounded. In particular for a point cloud varifold $V = \sum_{j=1}^{N} m_j \delta_{(x_j, P_j)}$ we obtain for $i \in \{1, \dots, N\}$

$$H_\varepsilon(x_i, V) = -\frac{d}{n\varepsilon} \frac{\displaystyle\sum_{j=1, j\neq i}^{N} m_j \rho'\left(\frac{|x_j - x_i|}{\varepsilon}\right) \Pi_{P_j}\left(\frac{x_j - x_i}{|x_j - x_i|}\right)}{\displaystyle\sum_{j=1}^{N} m_j \xi\left(\frac{|x_j - x_i|}{\varepsilon}\right)}.$$

In addition to consistency when $\varepsilon \to 0$, it is furthermore possible to state stability and convergence results with respect to a localized flat distance between varifolds (see [10], Thm. 4.3 and 4.5). When dealing with smooth objects, expression (3.3) can be modified in various ways preserving its consistency. In the rest of this section, we investigate several variants of approximate mean curvatures and establish their consistency with the classical mean curvature for smooth hypersurfaces in Proposition 3.3. While their is no significant benefit from considering those variants for computing an approximate curvature on a smooth hypersurface, they lead to numerical schemes for curvature flow behaving quite differently as shown in Sections 5.3 and 6.

More precisely, replacing Π_S in (3.2) by some linear operator $\Pi : \mathbb{R}^n \to \mathbb{R}^n$ that may depend on x_0, $x \in \mathbb{R}^n$ and $S \in G_{d,n}$ we introduce

$$H_\varepsilon^\Pi(x_0, V) = -\frac{d}{n\varepsilon} \frac{\displaystyle\int_{\mathbb{R}^n \times G_{d,n}} \rho'\left(\frac{|x - x_0|}{\varepsilon}\right) \frac{\Pi(x - x_0)}{|x - x_0|} \, dV(x, S)}{\displaystyle\int_{\mathbb{R}^n} \xi\left(\frac{|x - x_0|}{\varepsilon}\right) d\|V\|(x)}. \tag{3.4}$$

We will consider $\Pi \in \{\Pi_S, -2\,\Pi_{S^\perp}, 2\,\mathrm{Id}\}$, also post-composed with a projection onto the normal space at x_0. Notice that $\Pi = \Pi_S$ exactly corresponds to Definition 3.2. Moreover, the mean curvature of a C^2–submanifold M is a normal vector and post-composing with a projection onto the normal space $(T_{x_0}M)^\perp$ is then natural. We add that Brakke proved in [6] this orthogonality of the mean curvature vector extends to integral varifolds with locally bounded first variation.

Proposition 3.3 (Consistency for smooth varifolds)**.** *Assume $d = n - 1$ and let $M \subset \mathbb{R}^n$ be a d–submanifold of class C^2, whose mean curvature vector is denoted by $H : M \to \mathbb{R}^n$, and let $V = \mathcal{H}^d_{|M} \otimes \delta_{T_x M}$. Then, one obtains that*

$$H_\varepsilon^\Pi(x_0, V) \xrightarrow[\varepsilon \to 0]{} H(x_0).$$

for all $x_0 \in M$ and for $\Pi \in \{\Pi_S, -2\Pi_{S^\perp}, 2\mathrm{Id}\}$, and post-composed with $\Pi_{(T_{x_0}M)^\perp}$ for $\Pi \in \left\{\Pi_{(T_{x_0}M)^\perp} \circ \Pi_S, -2\Pi_{(T_{x_0}M)^\perp} \circ \Pi_{S^\perp}, 2\Pi_{(T_{x_0}M)^\perp}\right\}$. If M is at least C^3 then

$$\left|H_\varepsilon^\Pi(x_0, V) - H(x_0)\right| = O(\varepsilon).$$

Note that a corresponding result holds true for any codimension greater or equal than 1. Nevertheless, for the sake of simplicity and because we consider only the codimension 1 case in our numerical applications we state and prove the result only for $d = n - 1$.

Before we prove this proposition in the general case, let us depict the simplest case of a quadratic curve in $\mathbb{R}^2$. Taking into account $n\xi(s) = -s\rho(s)$ we obtain

$$H_\varepsilon(x_0, V) = \frac{\int_M \xi(\frac{x-x_0}{\varepsilon}) \frac{1}{|x-x_0|^2} \Pi(x - x_0)\, \mathrm{d}\mathcal{H}^1}{\int_M \xi(\frac{x-x_0}{\varepsilon})\, \mathrm{d}\mathcal{H}^1}$$

We define $M = \{x = (y, -ay^2) \,|\, y \in \mathbb{R}\}$ and set $x_0 = 0$. Then the normal on M is $\nu = \frac{(2ay,1)}{\sqrt{1+4a^2y^2}}$. For $\Pi = 2\mathrm{Id}$ we get $\frac{1}{|x|^2}\Pi x = \frac{(2y/y^2,-2a)}{(1+a^2y^2)}$ and thus using the symmetry in y we get $H_\varepsilon(x_0, V) = (0, -2a) + O(\varepsilon)$. For $\Pi = -2\Pi_{(T_xM)^\perp}$, one computes $\frac{1}{|x|^2}\Pi x = \frac{1}{y^2+a^2y^4}\frac{-2}{1+4a^2y^2}(4a^2y^3, ay^2) = \frac{1}{(1+a^2y^2)(1+4a^2y^2)}(-8a^2y, -2a)$ which again implies $H_\varepsilon(x_0, V) = (0, -2a) + O(\varepsilon)$. For $\Pi = \Pi_{T_xM}$, we can use that it is the average of $2\mathrm{Id}$ and $-2\Pi_{(T_xM)^\perp}$ and for the other choices of Π listed in the proposition analogous and easy computations lead to the same approximation result.

Proof. Up to an affine isometry, we can assume that $x_0 = 0$ and $T_{x_0}M = \mathbb{R}^{n-1} \times \{0\}$. We locally parametrize M by $u : \mathcal{U} \subset \mathbb{R}^{n-1} \to \mathbb{R}$ of class C^2 on an open set $\mathcal{U}$ containing 0. Consequently, for all $0 < \varepsilon < \varepsilon_0 \leq 1$ with ε_0 small enough,

$$M \cap B(0, \varepsilon) = \{(y, u(y)) \in \mathcal{U} \times \mathbb{R} : |y|^2 + |u(y)|^2 < \varepsilon^2\}$$

and $M \cap B(0, \varepsilon)$ is the graph of u over the open set $\mathcal{V}_\varepsilon = \{y \in \mathcal{U} : |y|^2 + |u(y)|^2 < \varepsilon^2\} \subset \mathbb{R}^{n-1}$. Thereby we have for the mean curvature $H(0) = \mathrm{trace}(D^2u(0))e_n$ with D^2u denoting the Hessian of u. Thanks to the following expansions

$$u(y) = \frac{1}{2}D^2u(0)y \cdot y + o(|y|^2) \quad \text{and} \quad \nabla u(y) = D^2u(0)y + o(|y|), \tag{3.5}$$

we have for the normal vector $\nu(y)$ to M at $(y, u(y)) \in M \cap B(0, \varepsilon)$,

$$\nu(y) = \frac{(\nabla u(y), -1)}{\sqrt{1 + |\nabla u(y)|^2}} = (1 + o(|y|)) \begin{pmatrix} D^2u(0)y + o(|y|) \\ -1 \end{pmatrix} = \begin{pmatrix} D^2u(0)y \\ -1 \end{pmatrix} + o(|y|). \tag{3.6}$$

By definition of the approximate mean curvature (3.4),

$$\left|H_\varepsilon^\Pi(0, V) - H(0)\right| = \frac{\left|\displaystyle\int_{\mathcal{V}_\varepsilon} f_\varepsilon(y, u(y))\sqrt{1 + |\nabla u(y)|^2}dy\right|}{\displaystyle\int_{\mathcal{V}_\varepsilon} \xi\left(\frac{|(y, u(y))|}{\varepsilon}\right)\sqrt{1 + |\nabla u(y)|^2}dy} \tag{3.7}$$

with $f_\varepsilon(z) = \dfrac{-(n-1)}{n\varepsilon}\rho'\left(\dfrac{|z|}{\varepsilon}\right)\dfrac{\Pi z}{|z|} - H(0)\xi\left(\dfrac{|z|}{\varepsilon}\right)$.

Up to decreasing ε_0 we can assume $D(0, \varepsilon_0) := \{y \in \mathbb{R}^{n-1} : |y| < \varepsilon_0\} \subset \mathcal{U}$. At first, we simplify the nominator and denominator *via* expansion of the area element and slightly enlarging the integration domain. Obviously, $\mathcal{V}_\varepsilon \subset D(0, \varepsilon)$ and there exists $\kappa > 0$ such that for all $y \in D(0, \varepsilon)$, $|u(y)| \leq \kappa|y|^2$. For $y \in \mathcal{U}$ and $|y| < \eta$ with $\eta = \varepsilon\sqrt{1 - \kappa^2\varepsilon^2}$ we obtain

$$|y|^2 + |u(y)|^2 < \eta^2 + \kappa^2\eta^4 = \varepsilon^2(1 - \kappa^2\varepsilon^2) + \kappa^2\varepsilon^4(1 - \kappa^2\varepsilon^2)^2 \leq \varepsilon^2,$$

which implies that $D(0,\eta) \subset \mathcal{V}_\varepsilon$. Moreover, notice that for g bounded and continuous on $D(0,\varepsilon)$, and using $D(0,\eta) \subset \mathcal{V}_\varepsilon \subset D(0,\varepsilon)$,

$$\left| \int_{D(0,\varepsilon)} g - \int_{\mathcal{V}_\varepsilon} g \right| \leq \sup_{D(0,\varepsilon)} |g| \, |D(0,\varepsilon) - \mathcal{V}_\varepsilon| \leq \sup_{D(0,\varepsilon)} |g| \, |D(0,\varepsilon) - D(0,\eta)|$$
$$= \sup_{D(0,\varepsilon)} |g| \, \omega_{n-1} \varepsilon^{n-1} \left(1 - (1 - (\kappa\varepsilon)^2)^{\frac{n-1}{2}} \right) = O(\varepsilon^{n+1}). \tag{3.8}$$

As $\rho'(|z|)\frac{z}{|z|} = \nabla(\rho(|z|))$ is uniformly bounded and $\|\Pi\| \leq 2$, we infer that the continuous map $\varepsilon f_\varepsilon((y,u(y)))\sqrt{1+|\nabla u(y)|^2}$ is uniformly bounded in $D(0,\varepsilon)$. Now, we apply (3.8) and due to $\sqrt{1+|\nabla u(y)|^2} = 1 + O(|y|^2)$ as well as $\varepsilon^{-1}\int_{D(0,\varepsilon)} O(|y|^2)dy = O(\varepsilon^n)$ deduce

$$\int_{\mathcal{V}_\varepsilon} f_\varepsilon((y,u(y)))\sqrt{1+|\nabla u(y)|^2}\, dy = \int_{D(0,\varepsilon)} f_\varepsilon((y,u(y)))\sqrt{1+|\nabla u(y)|^2}\, dy + \varepsilon^{-1} O(\varepsilon^{n+1})$$
$$= \int_{D(0,\varepsilon)} f_\varepsilon((y,u(y))\, dy + O(\varepsilon^n). \tag{3.9}$$

Analogously, we get for the denominator

$$\int_{\mathcal{V}_\varepsilon} \xi\left(\frac{|(y,u(y))|}{\varepsilon}\right)\sqrt{1+|\nabla u(y)|^2}\, dy = \int_{D(0,\varepsilon)} \xi\left(\frac{|(y,u(y))|}{\varepsilon}\right) dy + O(\varepsilon^{n+1}). \tag{3.10}$$

Next, we perform the expansion of kernels involved in (3.7). Thanks to (3.5) we deduce

$$|z| = |(y,u(y))| = \left(|y|^2 + |u(y)|^2\right)^{\frac{1}{2}} = \left(|y|^2 + O(|y|^4)\right)^{\frac{1}{2}} = |y|(1 + O(|y|^2))$$

so that for $y \in D(0,\varepsilon)$,

$$\xi\left(\frac{|z|}{\varepsilon}\right) = \xi\left(\frac{|y|}{\varepsilon} + \frac{|y|}{\varepsilon}O(|y|^2)\right) = \xi\left(\frac{|y|}{\varepsilon}\right) + \frac{|y|}{\varepsilon}O(|y|^2) = \xi\left(\frac{|y|}{\varepsilon}\right) + O(|y|^2)\,,$$
$$\frac{1}{|z|}\rho'\left(\frac{|z|}{\varepsilon}\right) = \frac{1}{|y| + O(|y|^3)}\left(\rho'\left(\frac{|y|}{\varepsilon}\right) + O(|y|^2)\right) = \frac{1}{|y|}\rho'\left(\frac{|y|}{\varepsilon}\right) + O(|y|).$$

It remains to expand Πz for $z = (y,u(y))$.

Case $\Pi = 2\mathrm{Id}$*:* We directly obtains $\Pi z = 2(y,u(y)) = \begin{pmatrix} 2y \\ D^2u(0)y\cdot y + o(|y|^2)\end{pmatrix}$.

Case $\Pi = -2\Pi_{(T_zM)^\perp}$*:* Using the expansion of the normal $\nu(y)$ from (3.6) we obtain

$$\begin{aligned}\Pi z &= -2(z\cdot\nu(y))\nu(y)\\ &= -2\left(\begin{pmatrix} y \\ \frac{1}{2}D^2u(0)y\cdot y + o(|y|^2)\end{pmatrix}\cdot\begin{pmatrix} D^2u(0)y + o(|y|) \\ -1 + o(|y|)\end{pmatrix}\right)\begin{pmatrix} D^2u(0)y + o(|y|) \\ -1 + o(|y|)\end{pmatrix}\\ &= -\left(D^2u(0)y\cdot y + o(|y|^2)\right)\begin{pmatrix} D^2u(0)y + o(|y|) \\ -1 + o(|y|)\end{pmatrix} = \begin{pmatrix} o(|y|^2) \\ D^2u(0)y\cdot y + o(|y|^2)\end{pmatrix}.\end{aligned}$$

Case $\Pi = \Pi_{T_zM}$*:* Taking into account the estimates in the previous two cases we achieve

$$\Pi z = \frac{1}{2}\left(2\mathrm{Id} - 2\Pi_{(\mathrm{T_zM})^\perp}\right) z = \begin{pmatrix} y + o(|y|^2) \\ D^2u(0)y\cdot y + o(|y|^2)\end{pmatrix}.$$

To summarize, in all three cases, we obtain

$$\Pi z \cdot e_i = \lambda y_i + o(|y|^2)\ \forall i \in \{1,\dots,n-1\} \quad \text{and} \quad \Pi z \cdot e_n = D^2u(0)y \cdot y + o(|y|^2), \tag{3.11}$$

with $\lambda = 2$ for $\Pi = 2\mathrm{Id}$, $\lambda = 0$ for $\Pi = -2\Pi_{(T_zM)^\perp}$, and $\lambda = 1$ for $\Pi = \Pi_{T_zM}$. Now, applying the co-area formula to the first term in the right hand side of (3.10) and using the above kernel expansions for $z = (y, u(y))$ we get

$$\begin{aligned}\int_{D(0,\varepsilon)} \xi\left(\frac{|z|}{\varepsilon}\right) dy &= \int_{D(0,\varepsilon)} \xi\left(\frac{|y|}{\varepsilon}\right) + O(|y|^2)\, dy \\ &= \int_{r=0}^{\varepsilon} \left(\xi\left(\frac{r}{\varepsilon}\right) + O(r^2)\right) \mathcal{H}^{n-2}\left(\partial D(0,r)\right)\, dr \\ &= \sigma_{n-2} \int_{r=0}^{\varepsilon} \xi\left(\frac{r}{\varepsilon}\right) r^{n-2}\, dr + O(\varepsilon^{n+1}),\end{aligned} \tag{3.12}$$

where $\sigma_{n-2} = (n-1)\omega_{n-1}$ is the area of the unit sphere in $\mathbb{R}^{n-1}$. Using (3.11) we obtain for $i \in \{1,\dots,n-1\}$,

$$\begin{aligned}\int_{D(0,\varepsilon)} \frac{1}{|z|}\rho'\left(\frac{|z|}{\varepsilon}\right) \Pi(z)\, dy \cdot e_i &= \int_{D(0,\varepsilon)} \left[\frac{1}{|y|}\rho\left(\frac{|y|}{\varepsilon}\right) + O(|y|)\right] (\lambda y_i + o(|y|^2))\, dy \\ &= \int_{r=0}^{\varepsilon} \left(\frac{1}{r}\rho'\left(\frac{r}{\varepsilon}\right) + O(r)\right) \int_{\partial D(0,r)} (\lambda y_i + o(r^2))\, d\mathcal{H}^{n-2}\, dr \\ &= \int_{r=0}^{\varepsilon} \left(\frac{1}{r}\rho'\left(\frac{r}{\varepsilon}\right) + O(r)\right) r^{n-2} o(r^2)\, dr = \int_{r=0}^{\varepsilon} o(r^{n-1}) dr \\ &= o(\varepsilon^n),\end{aligned} \tag{3.13}$$

where we used that $\displaystyle\int_{\partial D(0,r)} y_i\, d\mathcal{H}^{n-2}$ vanishes. Furthermore, using the kernel expansions and (3.11) we achieve

$$\begin{aligned}\int_{D(0,\varepsilon)} \frac{1}{|z|}\rho'\left(\frac{|z|}{\varepsilon}\right) \Pi(z)\, dy \cdot e_n &= \int_{r=0}^{\varepsilon} \left(\frac{1}{r}\rho'\left(\frac{r}{\varepsilon}\right) + O(r)\right) \int_{\partial D(0,r)} (D^2u(0)y \cdot y + o(r^2)) d\mathcal{H}^{n-2} dr \\ &= \int_{r=0}^{\varepsilon} \frac{1}{r}\rho'\left(\frac{r}{\varepsilon}\right) \int_{\partial D(0,r)} (D^2u(0)y \cdot y) d\mathcal{H}^{n-2} dr + o(\varepsilon^n).\end{aligned} \tag{3.14}$$

Next, we verify that $\displaystyle\int_{\partial D(0,r)} (D^2u(0)y \cdot y) d\mathcal{H}^{n-2} = H(0) \cdot e_n \frac{\sigma_{n-2}}{n-1} r^n$. Indeed, let $\{v_1,\dots,v_{n-1}\}$ be an orthonormal basis of $\mathbb{R}^{n-1}$ of eigenvectors of $D^2u(0)$ associated with eigenvalues $\kappa_1,\dots,\kappa_{n-1}$. Then decomposing $y = \displaystyle\sum_{j=1}^{n-1} \hat{y}_j v_i$ in $\mathcal{B}$, we have $D^2u(0)y \cdot y = \displaystyle\sum_{j=1}^{n-1} \kappa_j \hat{y}_j^2$ and by symmetry $\displaystyle\int_{\partial D(0,r)} \hat{y}_j^2\, dy = \frac{1}{n-1} \int_{\partial D(0,r)} |y|^2\, dy = \frac{\sigma_{n-2}}{n-1} r^n$. Hence, the claim follows from

$$\int_{\partial D(0,r)} (D^2u(0)y \cdot y) d\mathcal{H}^{n-2} = \sum_{j=1}^{n-1} \kappa_j \frac{\sigma_{n-2}}{n-1} r^n = \frac{\sigma_{n-2}}{n-1} r^n \operatorname{trace} D^2u(0). \tag{3.15}$$

Let $\Pi \in \{\Pi_S, -2\Pi_{S^\perp}, 2\mathrm{Id}\}$. Gathering the above estimates ((3.9) to (3.15)) and inserting them in (3.7), we conclude

$$\begin{aligned}
&\left|H_\varepsilon^{\Pi}\ (0,V) - H(0)\right| \\
&\quad= \left(\int_{r=0}^{\varepsilon} \xi\left(\frac{r}{\varepsilon}\right) r^{n-2}\, dr + O(\varepsilon^n)\right)^{-1} \left|H(0) \int_{r=0}^{\varepsilon} \left(\frac{1}{n}\frac{r}{\varepsilon}\rho'\left(\frac{r}{\varepsilon}\right) + \xi\left(\frac{r}{\varepsilon}\right)\right) r^{n-2}\, dr + o(\varepsilon^{n-1})\right| \\
&\quad= \frac{\varepsilon^{-(n-1)}}{C_\xi + O(\varepsilon)} \left(|H(0)|\varepsilon^{n-1} \int_{s=0}^{1} \left(\frac{1}{n} s\rho'(s) + \xi(s)\right) s^{n-2}\, ds + o(\varepsilon^{n-1})\right) \\
&\quad= 0 + o(1),
\end{aligned}$$

with $C_\xi = \displaystyle\int_{s=0}^{1} \xi(s) s^{n-2}\, ds$ and $\displaystyle\int_{s=0}^{1} \left(\frac{1}{n} s\rho'(s) + \xi(s)\right) s^{n-2}\, ds = 0$ by assumption (3.1).

As $H(0)$ is othogonal to T_0M, $\Pi_{(T_0M)^\perp} H(0) = H(0)$ and thus for $\Pi \in \{\Pi_S, -2\Pi_{S^\perp}, 2\mathrm{Id}\}$ we have

$$\left|\Pi_{(T_0M)^\perp} H_\varepsilon^{\Pi}(0,V) - H(0)\right| = o(1)\,.$$

Finally, it is straightforward to verify that for M being at least C^3 one obtains the improved convergence estimate $\left|H_\varepsilon^{\Pi}(0,V) - H(0)\right| = O(\varepsilon)$. □

In summary, consistency with the usual mean curvature holds for smooth varifolds (Prop. 3.3). In the particular case $\Pi = \Pi_S$, consistency with the generalized mean curvature holds almost everywhere (w.r.t. the mass measure) for rectifiable varifolds whose first variation is a Radon measure ([10]).

In view of stating convergence of approximate mean curvature $H_\varepsilon(\cdot, V_i)$ computed on point cloud varifolds $(V_i)_i$, when ε tends to 0 and V_i tends to a smooth (or rectifiable with first variation Radon) varifold, we tackle the stability issue in next section.

4. Stability of the approximate mean curvature

We are now going to state a quite general stability result (Thm. 4.8) on the approximate mean curvature introduced in (3.4). The stability will hold with respect to weak star convergence of varifolds, assuming that the limit varifold has finite mass and is *d–regular* in the sense that its mass $\|V\|$ is d–Ahlfors regular, *i.e.* there exists $C_0 \geq 1$, $r_0 > 0$ such that for all $x \in \operatorname{spt}\|V\|$ and $0 < r \leq r_0$,

$$C_0^{-1} r^d \leq \|V\|(B(x,r)) \leq C_0 r^d. \tag{4.1}$$

Note that r_0 can be chosen as large as needed: if condition (4.1) holds for some $r_0 > 0$ then it holds for any $r_1 \geq r_0$ possibly adapting the regularity constant C_0.

We now compare Theorem 4.8 with the main convergence result obtained in [10]: Theorem 5.5. The important contribution here is to get rid of thorny assumption (5.24) in Theorem 5.5 ([10]), this is the central issue in Section 4. Only relying on weak star convergence of varifolds, we are now able to prove convergence of approximate mean curvature. In doing so, we design a divergence between varifolds (4.5), that suitably adapts assumption (5.24) and tends to 0 (4.17), no longer as a reasonable though tricky assumption, but as a consequence of weak star convergence and Ahlfors regularity of the limit varifold. In Theorem 4.8, we also consider more general projector Π (as in (3.4)) than $\Pi = \Pi_S$ dealt with in [10]: this is easily achieved using the fact that the family of maps (indexed by $x \in \mathbb{R}^n$)

$$\Phi_x^\varepsilon : (y,S) \mapsto \frac{1}{\varepsilon}\rho'\left(\frac{|y-x|}{\varepsilon}\right) \frac{\Pi(y-x)}{|y-x|} = \Pi\nabla_y\left(\rho\left(\frac{|y-x|}{\varepsilon}\right)\right) \tag{4.2}$$

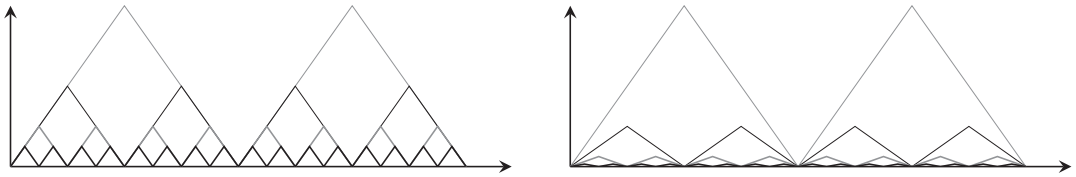

FIGURE 1. Two different sequences of curves C_ρ with different frequencies $\frac{1}{2\rho}$ and amplitude ρ^α for $\alpha = 1$ (left) and $\alpha = 2$ (right).

is equi-Lipschitz with Lipschitz constant bounded by $\varepsilon^{-2}\mathrm{Lip}(\rho')$. Our motivation for allowing more general projectors arises from numerical experiments: as we detail in Section 6, choosing $\Pi = \Pi_S$ leads to numerical instability of the scheme while other choices are better suited.

Theorem 4.8 requires some work on weak star and weak convergence of finite Radon measures as well as on the *flat distance* and *Prokhorov distance* that metrizes weak convergence (see Prop. 4.5 below).

The section is organized as follows, in a first part we introduce some material on weak and weak star convergences as well as *flat distance* and *Prokhorov distance*. In a second part we establish a general stability result (Prop. 4.7) holding in the neighborhood (with respect to aforementioned distances) of a d–regular varifold. Let us emphasize that d–regularity of a Radon measure is a weak assumption when it comes to prove stability for curvature estimates. In the third and last part, we put the results of the section together and state a convergence theorem (Thm. 4.8 and Cor. 4.9) for the approximate mean curvature (3.4) of a sequence of weak star converging varifolds.

All Radon measures we consider in this section are **nonnegative** (and nonzero) Radon measures.

4.1. Prokhorov and flat distance

Definition 4.1 (Weak and weak star convergence)**.** Let (X, d) be a locally compact and separable metric space (for us $X = \mathbb{R}^n$ or $X = \mathbb{R}^n \times G_{d,n}$) and let $(\mu_i)_{i\in\mathbb{N}}$, μ be Radon measures in X. We say that

(*i*) $(\mu_i)_i$ *weak star* converges to μ if for every $\varphi : X \to \mathbb{R}$ continuous and **compactly supported**, $\int \varphi d\mu_i \xrightarrow[i\to\infty]{} \int \varphi d\mu$.

(*ii*) If in addition the measures $(\mu_i)_i$, μ are finite, we say that $(\mu_i)_i$ *weak* converges to μ if for every $\varphi : X \to \mathbb{R}$ continuous and **bounded**, $\int \varphi d\mu_i \xrightarrow[i\to\infty]{} \int \varphi d\mu$.

Weak star convergence is also referred as vague convergence. By definition, weak convergence implies weak star convergence, whereas the converse is not true in general: compactly supported functions are blind to mass escaping at infinity or accumulating on the boundary. Consider for instance $\mu_i = \delta_i$ in $\mathbb{R}$ or $\mu_i = \delta_{\frac{1}{i}}$ in $]0, 1[$. In both cases μ_i weak star converge to 0 but does not weak converge.

A simple example of weak star convergence of varifolds is defined *via* a sequence of sawtooth type polygonal curves C_ρ of amplitude ρ^α for some $\alpha \geq 1$ and frequency $\frac{1}{2\rho}$ oscillating around the e_1 axis in $\mathbb{R}^2$ (*cf.* Fig. 1). Given these curves we define a sequence of varifolds V_ρ *via*

$$V_\rho(B) = (1 + \rho^{2(\alpha-1)})^{-\frac{1}{2}}\mathcal{H}^1(\{x \in C_\rho \,|\, (x, T_xC_\rho) \in B\}) \quad i.e. \quad V_\rho = (1 + \rho^{2(\alpha-1)})^{-\frac{1}{2}}\mathcal{H}^1_{|C_\rho} \otimes \delta_{T_xC_\rho}.$$

We denote by $D_{e_1} \subset \mathbb{R}^2$ the straight line along the e_1 axis. For $\alpha > 1$, the family (V_ρ) converges weak star for ρ tending to 0 to the varifold $V = \mathcal{H}^1_{D_{e_1}} \otimes \delta_{\mathrm{span}(e_1)}$ that is the smooth varifold associated with the straight line D_{e_1}. For $\alpha = 1$, the tangent direction alternates between $e_1 + e_2$ and $e_1 - e_2$ for any varifold V_ρ, the weak

star limit of the family of varifolds is $V = \mathcal{H}^1_{D_{e_1}} \otimes \frac{1}{2}\left(\delta_{\mathrm{span}(e_1+e_2)} + \delta_{\mathrm{span}(e_1-e_2)}\right)$, note that the measure in the Grassmannian is constant along the e_1 axis and consists of 2 atomic weights in the Grassmannian.

Note that finite Radon measures inherit the Banach structure of linear forms on $C_c(X)$ through Riesz representation theorem. However, the resulting total variation distance

$$d_{TV}(\mu,\nu) = |\mu-\nu|(X) = \sup\left\{ \int_X \varphi d\mu - \int_X \varphi d\nu \,\middle|\, \varphi \in \mathrm{C}_c(X), \sup|\varphi| \leq 1 \right\}$$

is much too strong with respect to compactness issues as well as approximation questions. Indeed, if x, $y \in X$ then whenever $x \neq y$, $d_{TV}(\delta_x, \delta_y) = 2$ no matter how small $d(x,y)$ is. Therefore, we introduce the so-called *flat distance* and *Prokhorov distance* that behave more consistently with weak and weak star topologies.

Definition 4.2 (Flat distance)**.** Let (X,d) be a locally compact and separable metric space (for us $X = \mathbb{R}^n$ or $X = \mathbb{R}^n \times G_{d,n}$) and let μ, ν be Radon measures. We define the (localized) *bounded Lipschitz distance* in the open set $U \subset X$:

$$\Delta_U(\mu,\nu) := \sup\left\{ \int_X \varphi \, d\mu - \int_X \varphi \, d\nu \,\middle|\, \begin{array}{l} \varphi \text{ is 1–Lipschitz} \\ \sup_X |\varphi| \leq 1 \\ \mathrm{spt}\,\varphi \subset U \end{array} \right\},$$

in the case $U = X$, we simply denote $\Delta = \Delta_X$. Note that Δ is a distance in the space of Radon measures.

For balls of radius less than 1, $\sup_X |\varphi| \leq 1$ is automatically satisfied in Definition 4.2.

Remark 4.3. Let V, W be d–varifolds in $\mathbb{R}^n$ and let $B \subset \mathbb{R}^n$ be an open set. We shorten $\Delta_{B\times G_{d,n}}(V,W)$ as $\Delta_B(V,W)$ and we observe that

$$\Delta_B(\|V\|,\|W\|) \leq \Delta_{B\times G_{d,n}}(V,W). \tag{4.3}$$

Indeed, let $\varphi \in \mathrm{C}_c(\mathbb{R}^n)$ be a 1–Lipschitz function supported in B and bounded by 1. On one hand $\psi : (y,S) \mapsto \varphi(y)$ is in particular a 1–Lipschitz function in $\mathrm{C}_c(\mathbb{R}^n \times G_{d,n})$ supported in $B \times G_{d,n}$ and bounded by 1. Furthermore, $\int_{\mathbb{R}^n} \varphi d\|V\| - \int_{\mathbb{R}^n} \varphi d\|W\| = \int_{\mathbb{R}^n\times G_{d,n}} \psi dV - \int_{\mathbb{R}^n\times G_{d,n}} \psi dW$ and (4.3) follows from Definition 4.2.

Definition 4.4 (Prokhorov distance)**.** Let μ, ν be finite Radon measures in $\mathbb{R}^n$ we recall that the *Prokhorov distance* is defined as

$$d_{\mathcal{P}}(\mu,\nu) := \inf\left\{ \delta > 0 \,\middle|\, \mu(A) \leq \nu(A^\delta) + \delta \text{ and } \nu(A) \leq \mu(A^\delta) + \delta, \forall A \subset X \text{ Borel set} \right\},$$

with $A^\delta = \bigcup_{x\in A} B(x,\delta)$. We introduce a slightly modified version of Prokhorov distance, for $d \in \mathbb{N}^*$,

$$\eta_d(\mu,\nu) := \inf\left\{ \delta > 0 \,\middle|\, \mu(B) \leq \nu(B^\delta) + \delta^d \text{ and } \nu(B) \leq \mu(B^\delta) + \delta^d, \forall B \subset \mathbb{R}^n \text{ closed ball} \right\}.$$

As Radon measures we work with are d–dimensional, homogeneity considerations lead to the modified Prokhorov distance η_d introduced in Definition 4.4. Notice that $\overline{A}^\delta = A^\delta$ for a Borel set $A \subset \mathbb{R}^n$ and then $\mu(A) \leq \mu(\overline{A}) \leq \nu(A^\delta) + \delta$ and it is natural to restrict to closed sets. Moreover, the restriction to balls is due to the convergence result we are interested in, nevertheless, as μ and ν are Radon measures in $\mathbb{R}^n$, if they coincide on balls then they are equal (thanks to Radon-Nikodym differentiation theorem for Radon measures) and thus η_d defines a distance among finite Radon measures. The triangular inequality is straightforward, using that $a^d + b^d \leq (a+b)^d$ for $a, b \geq 0$ and d a positive integer. The next proposition connects weak and weak star topologies and topology induced by both Prokhorov and flat distances.

Proposition 4.5. *Let (X,d) be a locally compact separable metric space (for us $X = \mathbb{R}^n$ or $X = \mathbb{R}^n \times G_{d,n}$) and let μ, $(\mu_i)_{i\in\mathbb{N}}$ be finite (nonzero) Radon measures.*

(1) $(\mu_i)_i$ *weak star converges to* μ *and* $\mu_i(X) \xrightarrow[i\to\infty]{} \mu(X)$ *if and only if* (μ_i) *weak converges to* μ.
(2) If $(\mu_i)_i$ *weak converges to* μ, *then both* $\Delta(\mu_i,\mu) \xrightarrow[i\to\infty]{} 0$ *and* $d_{\mathcal{P}}(\mu_i,\mu) \xrightarrow[i\to\infty]{} 0$.

We refer to [1][1.80] for the first point of Proposition 4.5 and Section 8.3 of [5] for the second point, let us mention that considering $\frac{\mu_i}{\mu_i(X)}$ and $\frac{\mu}{\mu(X)}$ allows to work with probability measures, for which the second point is more commonly stated. We now check that weak convergence implies convergence for η_d, which is all we need in this work.

Lemma 4.6. *Let* μ, ν *be finite Radon measures. Then*

$$\eta_d(\mu,\nu) \leq \begin{cases} (\Delta(\mu,\nu))^{\frac{1}{d+1}} & \text{if } \Delta(\mu,\nu) \leq 1 \\ (\Delta(\mu,\nu))^{\frac{1}{d}} & \text{if } \Delta(\mu,\nu) \geq 1 \end{cases}. \tag{4.4}$$

In particular, if $(\mu_i)_{i\in\mathbb{N}}$ *is a sequence of finite Radon measures weakly converging to* μ *then* $\eta_d(\mu_i,\mu)$ *tends to* 0 *when* $i \to \infty$.

Proof. The proof is standard, we give it for the sake of clarity. Let $B = \overline{B(x,r)} \subset \mathbb{R}^n$ and let $\varepsilon > 0$. We define $h_\varepsilon : \mathbb{R}_+ \to [0,1]$ and $\varphi_\varepsilon : \mathbb{R}^n \to [0,1]$ by

$$h_\varepsilon(t) = \begin{cases} 1 & \text{if } 0 \leq t \leq r \\ 0 & \text{if } t \geq r+\varepsilon \\ 1 - \frac{t-r}{\varepsilon} & \text{if } r < t < r+\varepsilon \end{cases} \qquad \text{and for } y \in \mathbb{R}^n,\ \varphi_\varepsilon(y) = h_\varepsilon(|y-x|)$$

so that φ_ε is radial, $\|\varphi_\varepsilon\|_\infty \leq 1$ and φ_ε is $\frac{1}{\varepsilon}$–Lipschitz. We infer that

$$\int \varphi_\varepsilon d\mu - \int \varphi_\varepsilon d\nu \leq \max\left(1, \frac{1}{\varepsilon}\right) \Delta(\mu,\nu).$$

Consequently,

$$\mu(B) \leq \int \varphi_\varepsilon d\mu \leq \int \varphi_\varepsilon d\nu + \max\left(1, \frac{1}{\varepsilon}\right) \Delta(\mu,\nu) \leq \nu(B^\varepsilon) + \max\left(1, \frac{1}{\varepsilon}\right) \Delta(\mu,\nu).$$

If $\Delta(\mu,\nu) \geq 1$, we can take $\varepsilon = (\Delta(\mu,\nu))^{\frac{1}{d}} \geq 1$ and we obtain $\eta_d(\mu,\nu) \leq (\Delta(\mu,\nu))^{\frac{1}{d}}$. If $\Delta(\mu,\nu) \leq 1$, we can take $\varepsilon = (\Delta(\mu,\nu))^{\frac{1}{d+1}} \leq 1$ and we obtain $\eta_d(\mu,\nu) \leq (\Delta(\mu,\nu))^{\frac{1}{d+1}}$.
The last part of the statement follows from second point of Proposition 4.5. □

4.2. A stability result

Unfortunately, stability of the approximate mean curvature does not hold directly with respect to Prokhorov or flat distance but with respect to a combination $\delta(\cdot,\cdot)$ of both that is not a distance, defined in (4.5) below. Nevertheless, we prove in Theorem 4.8 *(i)* that $\delta(V,V_i)$ tends to 0 when the sequence of varifolds $(V_i)_i$ weak star converge to a d–regular varifold V. We define for V, W two d–varifolds in $\mathbb{R}^n$,

$$\delta(V,W) = \sup\left\{ \frac{\Delta_B(V,W)}{(\eta_d(\|V\|,\|W\|) + \mathrm{diam}B/2)^d} \,\middle|\, B \subset \mathbb{R}^n \text{ ball centered in } \operatorname{spt}\|V\| \right\}. \tag{4.5}$$

Proposition 4.7. *Let* V *be a* d*–regular varifold in* $\mathbb{R}^n$ *of finite mass, let* $x \in \operatorname{spt}\|V\|$ *and let* $\varepsilon \in]0,1[$. *Then for any* d*–varifold* W *and* $z \in \mathbb{R}^n$ *satisfying*

$$|x-z| + \eta_d(\|V\|,\|W\|) \leq \gamma\varepsilon \quad \textit{with} \quad \gamma = \frac{1}{8\left(1 + 2C_0^{\frac{1}{d}} + C_0^{\frac{2}{d}}\right)}, \tag{4.6}$$

where $C_0 \geq 1$ is the d–regularity constant from (4.1), we have

$$\left|H^\Pi_\varepsilon(z,W) - H^\Pi_\varepsilon(x,V)\right| \leq C\frac{\delta(V,W)+|x-z|}{\varepsilon^2}, \tag{4.7}$$

where $C>0$ only depends on d, n, C_0, ξ and ρ.

Proof. We shorten notations $\eta := \eta_d(\|V\|,\|W\|)$ and $\delta := \delta(V,W)$ and $B = B(x,\varepsilon+|x-z|)$. We apply Definition 4.2 of Δ_B together with the fact that $\xi\left(\frac{|\cdot|}{\varepsilon}\right)$ is $\frac{\mathrm{Lip}(\xi)}{\varepsilon}$–Lipschitz to obtain

$$\begin{aligned}
\varepsilon^n&\left|\|W\|*\xi_\varepsilon(z) - \|V\|*\xi_\varepsilon(x)\right| \\
&\leq \left|\int \xi\left(\frac{|\cdot-z|}{\varepsilon}\right) d\|W\| - \int \xi\left(\frac{|\cdot-z|}{\varepsilon}\right) d\|V\|\right| + \int \left|\xi\left(\frac{|\cdot-z|}{\varepsilon}\right) - \xi\left(\frac{|\cdot-x|}{\varepsilon}\right)\right| d\|V\| \\
&\leq \frac{\mathrm{Lip}(\xi)}{\varepsilon}\left(\Delta_B(\|W\|,\|V\|) + |x-z|\|V\|(B)\right).
\end{aligned} \tag{4.8}$$

From (4.8), Remark 4.3 and d–regularity of $\|V\|$ (4.1), we infer

$$\begin{aligned}
\varepsilon^n\left|\|W\|*\xi_\varepsilon(z) - \|V\|*\xi_\varepsilon(x)\right| &\leq \frac{\mathrm{Lip}(\xi)}{\varepsilon}\left(\Delta_B(W,V) + C_0|x-z|\left(\varepsilon+|x-z|\right)^d\right) \\
&\leq \frac{\mathrm{Lip}(\xi)}{\varepsilon}\left(\delta\left(\varepsilon+|x-z|+\eta\right)^d + C_0|x-z|\left(\varepsilon+|x-z|\right)^d\right) \text{ by (4.5)} \\
&\leq C_0\mathrm{Lip}(\xi)\frac{\delta+|x-z|}{\varepsilon}\left(\varepsilon+|x-z|+\eta\right)^d \\
&\leq C_1\frac{\delta+|x-z|}{\varepsilon}\varepsilon^d
\end{aligned} \tag{4.9}$$

with $C_1 := 2^d C_0\mathrm{Lip}(\xi)$ using $\varepsilon+|x-z|+\eta \leq 2\varepsilon$. We repeat the same argument with Φ^ε_x defined in (4.2), $\mathrm{Lip}(\Phi^\varepsilon_z) \leq \varepsilon^{-2}\mathrm{Lip}(\rho')$ and then

$$\begin{aligned}
\left|\int_{\mathbb{R}^n\times G_{d,n}} \Phi^\varepsilon_z\, dW - \int_{\mathbb{R}^n\times G_{d,n}} \Phi^\varepsilon_x\, dV\right| &\leq \frac{\mathrm{Lip}(\rho')}{\varepsilon^2}\left(\Delta_B(W,V) + |x-z|\|V\|(B)\right) \\
&\leq C_2\frac{\delta+|x-z|}{\varepsilon^2}\varepsilon^d \quad \text{with} \quad C_2 := 2^d C_0\mathrm{Lip}(\rho')
\end{aligned} \tag{4.10}$$

Last but not least, we estimate $\varepsilon^n\|W\|*\xi_\varepsilon(z)$ from below thanks to the mass $\|V\|$ of rings of radii comparable to ε. Recall that ξ is positive in $(0,1)$ and denote $\beta = \min\left\{\xi(s)\,\middle|\, s\in\left[\frac{C_0^{-2/d}}{4},\frac{1}{2}\right]\right\} > 0$. We then have,

$$\begin{aligned}
\varepsilon^n\|W\|*\xi_\varepsilon(z) &= \int \xi\left(\frac{|y-z|}{\varepsilon}\right) d\|W\|(y) \geq \beta\,\|W\|\left(B(z,\tfrac{\varepsilon}{2})) \setminus \overline{B(z,C_0^{-2/d}\tfrac{\varepsilon}{4})}\right) \\
&\geq \beta\left(\|W\|(B(z,\tfrac{\varepsilon}{2})) - \|W\|(B(z,C_0^{-2/d}\tfrac{\varepsilon}{4})\right).
\end{aligned} \tag{4.11}$$

From (4.11), we first apply Definition 4.4 of η, then we use the inclusion of balls $B(x, R-|x-z|) \subset B(z,R) \subset B(x, R+|x-z|)$ for a given radius $R > |x-z|$ and we finally get (4.12) thanks to the d–regularity of $\|V\|$ (4.1):

$$\begin{aligned}
\varepsilon^n \|W\| * \xi_\varepsilon(z) &\geq \beta \left(\left[\|V\|(B(z, \tfrac{\varepsilon}{2} - \eta)) - \eta^d \right] - \left[\|V\|(B(z, C_0^{-2/d} \tfrac{\varepsilon}{4} + \eta)) + \eta^d \right] \right) \\
&\geq \beta \left(\|V\|(B(x, \tfrac{\varepsilon}{2} - (\eta + |x-z|))) - \|V\|(B(x, C_0^{-2/d} \tfrac{\varepsilon}{4} + (\eta + |x-z|))) - 2\eta^d \right) \\
&\geq \beta \left(C_0^{-1} 2^{-d} (\varepsilon - 2(\eta + |x-z|))^d - C_0 2^{-d} \left(C_0^{-2/d} \frac{\varepsilon}{2} + 2(\eta + |x-z|) \right)^d - 2\eta^d \right) \\
&\geq \beta C_0^{-1} 2^{-d} \underbrace{\left((\varepsilon - 2(\eta + |x-z|))^d - (\frac{\varepsilon}{2} + 2C_0^{2/d}(\eta + |x-z|))^d - (2(2C_0)^{1/d}\eta)^d \right)}_{=:A}. \qquad (4.12)
\end{aligned}$$

Using once again that $a^d + b^d \leq (a+b)^d$ for $a, b \geq 0$ we estimate A as follows:

$$A \geq (\varepsilon - 2(\eta + |x-z|))^d - \left(\frac{\varepsilon}{2} + 2C_0^{2/d}(\eta + |x-z|) + 2(2C_0)^{1/d}\eta \right)^d$$

and then using that for $a \geq b \geq 0$, $a^d - b^d \geq (a-b)a^{d-1}$ with $a = \varepsilon - 2(\eta + |x-z|)$ and $b = \frac{\varepsilon}{2} + 2C_0^{2/d}(\eta + |x-z|) + 2(2C_0)^{1/d}\eta$, we get

$$A \geq \underbrace{\frac{1}{2} \left(\varepsilon - 4(1 + (2C_0)^{1/d} + C_0^{2/d})(\eta + |x-z|) \right)}_{\geq \frac{1}{2}\left(\frac{\varepsilon}{2}\right)^d \text{ by assumption in (4.6)}} (\varepsilon - 2(\eta + |x-z|))^{d-1}.$$

We conclude that

$$\varepsilon^n \|W\| * \xi_\varepsilon(z) \geq C_3^{-1} \varepsilon^d \quad \text{with} \quad C_3 = \beta^{-1} C_0 2^{2d+1} \qquad (4.13)$$

We similarly have

$$\varepsilon^n \|V\| * \xi_\varepsilon(x) \geq C_3^{-1} \varepsilon^d. \qquad (4.14)$$

Eventually, for Π as in (3.4) and using $\|\Pi\| \leq 2$ and (4.1),

$$\begin{aligned}
\left| \int \Phi_x^\varepsilon dV \right| &\leq \int_{B(x,\varepsilon) \times G_{d,n}} \frac{1}{\varepsilon} \left| \rho' \left(\frac{|y-x|}{\varepsilon} \right) \frac{\Pi(y-x)}{|y-x|} \right| dV(y,S) \leq \frac{2}{\varepsilon} \|\rho'\|_\infty \|V\|(B(x,\varepsilon)) \\
&\leq \frac{2}{\varepsilon} \|\rho'\|_\infty C_0 \varepsilon^d \leq C_4 \varepsilon^{d-1} \quad \text{with } C_4 := 2C_0 \|\rho'\|_\infty \qquad (4.15)
\end{aligned}$$

We combine (4.9), (4.10), (4.13), (4.14) and (4.15) so that

$$\begin{aligned}
\left| H_\varepsilon^\Pi(z,W) - H_\varepsilon^\Pi(x,V) \right| &= \left| \frac{\int \Phi_z^\varepsilon \, dW}{\varepsilon^n \|W\| * \xi_\varepsilon(z)} - \frac{\int \Phi_x^\varepsilon \, dV}{\varepsilon^n \|V\| * \xi_\varepsilon(x)} \right| \\
&\leq \frac{1}{\varepsilon^n \|W\| * \xi_\varepsilon(z)} \left(\left| \int \Phi_z^\varepsilon \, dW - \int \Phi_x^\varepsilon \, dV \right| \right. \\
&\qquad \left. + \frac{\left| \int \Phi_x^\varepsilon dV \right|}{\varepsilon^n \|V\| * \xi_\varepsilon(x)} \varepsilon^n \left| \|W\| * \xi_\varepsilon(z) - \|V\| * \xi_\varepsilon(x) \right| \right) \\
&\leq C_3 \varepsilon^{-d} \left(C_2 \frac{\delta + |x-z|}{\varepsilon^2} \varepsilon^d + C_3 \varepsilon^{-d} C_4 \varepsilon^{d-1} C_1 \frac{\delta + |x-z|}{\varepsilon} \varepsilon^d \right) \\
&\leq C_3 \left(C_2 + C_1 C_3 C_4 \right) \frac{\delta + |x-z|}{\varepsilon^2},
\end{aligned}$$

and $C = C_3\,(C_2 + C_1C_3C_4) > 0$ is then a constant depending on d, n, C_0, ρ and ξ and in particular uniform w.r.t. x. □

In order to establish convergence of approximate mean curvature under weak star convergence of varifolds, it remains to prove that $\delta(V, V_i)$ tends to 0 when V_i weak star converges to V, which is the key point of the end of the section.

4.3. Convergence of approximate mean curvature

Let us transfer the measure setting introduced in Section 4.1 to our varifolds framework $X = \mathbb{R}^n \times G_{d,n}$. For a d–varifold V, the total variation is $V(X) = V(\mathbb{R}^n \times G_{d,n}) = \|V\|(\mathbb{R}^n)$. Let $(V_i)_{i\in\mathbb{N}}$, V be d–varifolds such that $(V_i)_i$ weak star converges to V, with $\|V\|(\mathbb{R}^n) < +\infty$ and with support contained in a fixed compact $K \times G_{d,n} \subset \mathbb{R}^n \times G_{d,n}$. Then, $\|V_i\|$ weak star converges to $\|V\|$ and moreover $\|V_i\|(\mathbb{R}^n) \to \|V\|(\mathbb{R}^n)$. Indeed, $\|V\|(\mathbb{R}^n) \leq \liminf_{i\to\infty} \|V_i\|(\mathbb{R}^n)$ by lower semi continuity of total variation. And in addition, as all V_i are supported in the same compact set $K \times G_{d,n}$, we have that

$$\limsup_{i\to\infty} \|V_i\|(\mathbb{R}^n) = \limsup_{i\to\infty} V_i(K \times G_{d,n}) \leq V(K \times G_{d,n}) = \|V\|(\mathbb{R}^n),$$

hence $\lim_{i\to\infty} \|V_i\|(\mathbb{R}^n) = \|V\|(\mathbb{R}^n) < +\infty$. Consequently, thanks to Proposition 4.5, $(V_i)_i$ (resp. $(\|V_i\|)_i$) weak converges to V (resp. $\|V\|$) and both

$$\sup_{B\subset\mathbb{R}^n \text{ ball}} \Delta_B(V, V_i) \leq \Delta(V, V_i) \xrightarrow[i\to\infty]{} 0 \quad \text{and} \quad \eta_d(\|V_i\|, \|V\|) \xrightarrow[i\to\infty]{} 0 \text{ hold.} \tag{4.16}$$

Theorem 4.8. *Let V be a d–regular varifold in $\mathbb{R}^n$ with regularity constant $C_0 \geq 1$ in (4.1) and assume $\|V\|(\mathbb{R}^n) < \infty$. Let $(V_i)_i$ be a sequence of d–varifolds weak star converging to V. Assume that there exists a compact set $K \subset \mathbb{R}^n$ such that $\operatorname{spt} V_i \subset K \times G_{d,n}$ for all i. Then,*

(i) setting $d_i := \delta(V, V_i)$ (δ has been defined in (4.5)) we have

$$d_i \to 0 \quad \text{for } i \to \infty; \tag{4.17}$$

(ii) setting $\eta_i := \eta_d(\|V\|, \|V_i\|)$, there exists a constant $C > 0$ depending only on d, n, C_0, ξ and ρ such that: if $x \in \operatorname{spt}\|V\|$ and $(z_i)_i \subset \mathbb{R}^n$ converges to x, then for any sequence $(\varepsilon_i)_i \subset]0,1[$ tending to 0 and satisfying

$$|x - z_i| + \eta_i \leq \gamma\varepsilon_i, \quad \text{for} \quad \gamma = \left(8(1 + (2C_0)^{1/d} + C_0^{2/d})\right)^{-1} \tag{4.18}$$

we have

$$\left|H^{\Pi}_{\varepsilon_i}(z_i, V_i) - H^{\Pi}_{\varepsilon_i}(x, V)\right| \leq C\frac{d_i + |x - z_i|}{\varepsilon_i^2}. \tag{4.19}$$

Note that (ii) directly follows from Proposition 4.7, and (i) again holds under the flexible assumption that V is d–regular in the sense of (4.1).

Proof. Proof of (i): We first show that $d_i \to 0$.
As varifolds are supported in the same compact set $K \times G_{d,n}$, we have (4.16), *i.e.*

1. $(V_i)_i$ weak converges to V and the flat distance $\Delta(V, V_i)$ tends to 0, thus
$$\sup_{B\subset\mathbb{R}^n \text{ ball}} \Delta_B(V, V_i) \leq \Delta(V, V_i) \xrightarrow[i\to\infty]{} 0,$$
2. $(\|V_i\|)_i$ weak converge to $\|V\|$ and both $\Delta(\|V_i\|, \|V\|) \xrightarrow[i\to\infty]{} 0$ and $\eta_i := \eta_d(\|V_i\|, \|V\|) \xrightarrow[i\to\infty]{} 0$.

Let us argue by contradiction and, up to extraction of a subsequence, assume that $\exists \bar{\delta} > 0$ such that $\forall i \in \mathbb{N}$, $d_i > \bar{\delta}$. By definition of d_i, there is a sequence of balls $(B_i)_i \subset \mathbb{R}^n$, $B_i = B(x_i, r_i)$ with $x_i \in \operatorname{spt}\|V\|$ and $r_i > 0$, such that for all i,

$$\Delta_{B_i}(V, V_i) > \bar{\delta}(r_i + \eta_i)^d.$$

And we already know that $\Delta_{B_i}(V_i, V) \leq \Delta(V, V_i) \xrightarrow[i\to\infty]{} 0$, thus $(r_i+\eta_i)^d$ must tend to 0 as well, and η_i already tends to 0 so that we eventually conclude that $r_i \xrightarrow[i\to\infty]{} 0$.

Now, from the definition of Δ_{B_i}, $\Delta_{B_i}(V, V_i) > \bar{\delta}(r_i + \eta_i)^d$ implies that there exists a sequence of 1–Lipschitz functions $(\varphi_i)_i \in \mathrm{C}(\mathbb{R}^n \times G_{d,n})$ with $\operatorname{spt}\varphi_i \subset B_i$, $\|\varphi_i\|_\infty \leq 1$ and such that for all i,

$$\left| \int_{B_i \times G_{d,n}} \varphi_i dV_i - \int_{B_i \times G_{d,n}} \varphi_i dV \right| > \bar{\delta}(r_i + \eta_i)^d. \tag{4.20}$$

Applying Ascoli compactness theorem in $\mathrm{C}(K \times G_{d,n})$, up to extracting a subsequence, there exists a continuous function $\varphi \in \mathrm{C}(K \times G_{d,n})$ such that $\varphi_i \xrightarrow[i\to\infty]{} \varphi$ uniformly in $K \times G_{d,n}$.

It is not difficult to see that $\varphi = 0$. Indeed, let us consider

$$X = \{y \in K : |\varphi(y)| > 0\}.$$

Let $x \in X$, then $\exists N = N_x \in \mathbb{N}$ such that for all $i \geq N$, $|\varphi_i(x)| > 0$ and thus $x \in B_i$. Therefore, $|x - x_i| \leq r_i \xrightarrow[i\to\infty]{} 0$ and thus, $(x_i)_i$ converges to x. Consequently X contains at most one point and on the other hand X is open by continuity of φ so that $X = \emptyset$.

Coming back to (4.20) we first get by definition of η_i that $\|V_i\|(B_i) \leq \|V\|(B_i^{\eta_i}) + (\eta_i)^d$ and then by (4.1)

$$\begin{aligned}\bar{\delta}(r_i + \eta_i)^d &< \sup_{K\times G_{d,n}} |\varphi_i| \left(\|V_i\|(B_i) + \|V\|(B_i)\right) \leq \left(C_0(r_i+\eta_i)^d + (\eta_i)^d + C_0(r_i)^d\right) \sup_{K\times G_{d,n}} |\varphi_i| \\ &\leq 2C_0(r_i + \eta_i)^d \sup_{K\times G_{d,n}} |\varphi_i|.\end{aligned}$$

It follows that, $0 < \bar{\delta} < \dfrac{2C_0(r_i+\eta_i)^d}{(r_i+\eta_i)^d} \sup_{K\times G_{d,n}} |\varphi_i| \leq 2C_0 \sup_{K\times G_{d,n}} |\varphi_i|$ leading to a contradiction since $\sup_{K\times G_{d,n}} |\varphi_i| \xrightarrow[i\to\infty]{} \sup_{K\times G_{d,n}} |\varphi| = 0$.

Proof of (ii): apply Proposition 4.7 with $W = V_i$. □

Eventually combining consistency (Prop. 3.3) and stability (Thm. 4.8) we obtain the convergence of the approximate mean curvature. The following result (Cor. 4.9) is a particular case where strong regularity of the limit varifold ensures that assumptions of both consistency and stability are fulfilled. However, the C^3 regularity assumption is stronger than necessary and more general results essentially require to check that Proposition 3.3 and stability Theorem 4.8 apply.

Corollary 4.9 (Convergence)**.** *Let V be a d–varifold associated with a compact d–submanifold $M \subset \mathbb{R}^n$ without boundary of class C^3. Let $(V_i)_i$ be a sequence of d–varifolds weak star converging to V. Assume that there exists a compact set $K \subset \mathbb{R}^n$ such that $\operatorname{spt} V_i \subset K \times G_{d,n}$ for all i. Then, define $d_i = \delta(V, V_i)$ (as in (4.5)) and let $x \in M$, $(z_i)_i \subset \mathbb{R}^n$ such that $|x - z_i| \to 0$, for any sequence $(\varepsilon_i)_i \subset (0,1)$ tending to 0 and satisfying $|x - z_i| + \eta_d(\|V\|, \|V_i\|) = o(\varepsilon_i)$ we have*

$$\begin{aligned}\left|H^{\Pi}_{\varepsilon_i}(z_i, V_i) - H(x, V)\right| &= O\left(\frac{d_i + |x - z_i|}{\varepsilon_i^2}\right) + O(\varepsilon_i) \\ &\xrightarrow[i\to\infty]{} 0 \quad \textit{as soon as } \sqrt{d_i + |x - z_i|} = o(\varepsilon_i).\end{aligned}$$

Proof. First of all, we recall that a closed d–submanifold of $\mathbb{R}^n$ of class C^2 is in particular d–regular and then $\exists C_0 \geq 1$ such that for all $x \in M$ and $0 < r \leq \mathrm{diam} M$,

$$C_0^{-1} r^d \leq \|V\|(B(x,r)) = \mathcal{H}^d(M \cap B(x,r)) \leq C_0 r^d.$$

We mention that one could adapt the proof of Proposition 3.3 and more precisely apply (3.8) with $g = \sqrt{1+|\nabla u|^2}$ to infer the d–regularity of M. Applying Theorem 4.8 and Proposition 3.3 (in particular the last estimate for M being at least C^3) to

$$\left|H^{\Pi}_{\varepsilon_i}(z_i, V_i) - H(x,V)\right| \leq \left|H^{\Pi}_{\varepsilon_i}(z_i, V_i) - H^{\Pi}_{\varepsilon_i}(x,V)\right| + \left|H^{\Pi}_{\varepsilon_i}(x,V) - H(x,V)\right|$$

concludes the proof. □

In the case of a point cloud varifold $V = \sum_{i=1}^N m_i \delta_{(x_i, P_i)}$, and for

$$\Pi = \Pi_{ij} \in \{\Pi_{P_j},\ -2\Pi_{P_j^\perp},\ 2\,\mathrm{Id},\ \Pi_{P_i^\perp} \circ \Pi_{P_j},\ -2\Pi_{P_i^\perp} \circ \Pi_{P_j^\perp},\ 2\Pi_{P_j^\perp}\} \tag{4.21}$$

we rewrite the approximate mean curvature

$$H^{\Pi}_{\varepsilon}(x_i, V) = -\frac{d}{n}\frac{1}{\varepsilon} \frac{\displaystyle\sum_{j=1}^N m_j \rho'\left(\frac{|x_j - x_i|}{\varepsilon}\right) \Pi_{ij}\left(\frac{x_j - x_i}{|x_j - x_i|}\right)}{\displaystyle\sum_{j=1}^N m_j \xi\left(\frac{|x_j - x_i|}{\varepsilon}\right)}. \tag{4.22}$$

Proposition 3.3 leaves us with at least 6 possible choices for the definition of an approximate mean curvature, more or less equivalently reasonable in the continuous smooth case. Our numerical experiments in Section 6 indicate that those formulas can behave very differently when used in the context of a time discretization for the simulation of mean curvature flows.

Remark 4.10 (k–nearest neighbors)**.** Notice that in the use of formula (4.22), it is advisable to ensure that the selected neighbourhood is sufficiently large and contains at least a fixed number of points. This is an appropriate procedure especially for point clouds that are not uniformly sampled. In fact, for point clouds of moderate density we prescribe the number k of nearest points to be considered and infer ε so that the support of $\rho\left(\frac{|\cdot - x_i|}{\varepsilon}\right)$ exactly contains x_i plus $k-1$ other points.

5. Mean curvature motion and comparison principles

5.1. Computation of masses and directions for point cloud varifolds

Before we discuss the actual time discretization let us detail how we derive masses and directions from positions. In the case of a smooth varifold $V = \mathcal{H}^d_{|M} \otimes \delta_{T_x M}$ associated with a d–submanifold $M \subset \mathbb{R}^n$, the tangent plane and the varifold are completely determined by the knowledge of M. In the case of a point cloud varifold, there is no unique choice of masses $\{m_i\}_{i=1}^N$ and sets of directions $\{P_i\}_{i=1}^N$. Here, we will follow standard approaches. The ansatz to define the masses m_i is as follows. We assume that the positions $\{x_i\}_i$ are close to some d–submanifold M and we want to define masses $\{m_i\}_i$ such that the resulting Radon measures $\mu := \sum_{i=1}^N m_i \delta_{x_i}$ and $\nu := \mathcal{H}^d_{|M}$ are close in the sense of measures. To this end, we regularize μ and ν *via* convolution. *I.e.* we define $\lambda_\delta(x) = \delta^{-n}\lambda(|x|/\delta)$ for $\lambda : \mathbb{R} \to \mathbb{R}$ nonnegative, even, and compactly supported in $[-1,1]$. Then we renormalize the regularized μ by the regularized ν in the sense that

$$m_i = \frac{\nu * \lambda_\delta(x_i)}{\mu * \lambda_\delta(x_i)}$$

Unfortunately, M and thus ν are not known and we replace $\delta^n \nu * \lambda_\delta(x_i)$ with its first order approximation $C_\lambda \delta^d$ with $C_\lambda = \int_{\mathbb{R}^d} \lambda(|y|)\, dy = \sigma_{d-1} \int_{s=0}^1 \lambda(s) s^{d-1}\, ds$ being the volume weighted by λ of the unit ball in $\mathbb{R}^d$. From this we deduce for the masses

$$m_i = \frac{C_\lambda \delta^d}{\displaystyle\sum_{j=1}^N \lambda\left(\frac{|x_j - x_i|}{\delta}\right)}.$$

To the best of our knowledge, there is unfortunately no general result of convergence of such estimators, assuming for instance a control of the Hausdorff distance between M and $\{x_i\}_i$ and asking for $\{m_i\}_i$ ensuring that μ and ν are close in flat distance or in Wasserstein type distance. In our numerical experiments, we will consider either λ smooth and compactly supported or $\lambda = \chi_{]-1,1[}$ which implies

$$m_i = \frac{\omega_d \delta^d}{k_\delta} \quad \text{with} \quad k_\delta = \operatorname{card}\{j \in \{1, \dots, N\} : |x_j - x_i| < \delta\}.$$

As it is usually done, sets of directions $\{P_i\}_i$ are computed through a local weighted linear regression. We fix a further nonnegative and even profile kernel $\zeta : \mathbb{R} \to \mathbb{R}$ supported in $]-1,1[$ and a sufficiently large parameter $\sigma > 0$ and define, based on a σ–neighborhood of some point x_i containing k_σ points, a center of mass

$$\bar{x} = \frac{1}{k_\sigma} \sum_{j=1}^N \chi_{]-1,1[}\left(\frac{|x_j - x_i|}{\sigma}\right) x_j$$

of the points σ–close to the point x_i. Furthermore, with the notation $x = (x^{(1)}, \dots, x^{(n)})$ for the n–components of $x \in \mathbb{R}^n$, we compute the n by n covariance matrix $M^i = (M^i_{kl})_{k,l=1,\dots n}$ of coefficient (k,l):

$$M^i_{kl} = \sum_{j=1}^N \zeta\left(\frac{|x_j - x_i|}{\sigma}\right)\left(x_j^{(k)} - \bar{x}^{(k)}\right)\left(x_j^{(l)} - \bar{x}^{(l)}\right).$$

The matrix M^i is symmetric and positive semi-definite. The d eigenvectors associated with the d highest eigenvalues provide a basis of an approximate tangent space P_i and the $(n-d)$ eigenvectors corresponding to the $(n-d)$ smallest eigenvalues provide a basis of an approximate normal space $P_i^\perp$. When using a smooth profile ζ, this way of computing tangent plane ensures its spatial regularity. In our numerical experiments, we have chosen $\zeta = \xi$ smooth and compactly supported in $]-1,1[$. As pointed out in Remark 4.10 concerning ε, for practical reasons it is advisable to fix $(k_\varepsilon, k_\sigma, k_\delta)$ and to define $(\varepsilon, \sigma, \delta)$ accordingly (as the radius of the smallest ball containing the right number of nearest points), in this case $(\varepsilon, \sigma, \delta)$ vary, depending on the sampling of the point cloud. This is what we finally have used in the applications.

5.2. Time continuous mean curvature motion and comparison principles

Now, we are in the position to formulate mean curvature motion for point cloud varifolds. More precisely, given a point cloud d–varifold $V = \sum_{i=1\dots,N} m_i \delta_{(x_i,P_i)}$ in $\mathbb{R}^n$, we consider the following system of ordinary differential equations:

Find a family of varifolds $(V(t))_{t\geq 0}$ with

$$V(t) = \sum_{i=1}^N m_i(X(t)) \delta_{(x_i(t), P_i(X(t)))} \quad \text{and} \quad X(t) = (x_1(t), \dots, x_N(t)) \in \mathbb{R}^{nN}$$

such that

$$\tfrac{\mathrm{d}}{\mathrm{d}t} x_i(t) = H^\Pi_\varepsilon(x_i(t), V(t)) \tag{5.1}$$

for prescribed initial data $V(0) = V$ and $i = 1 \dots N$. Here, $m_i(X(t))$ and $P_i(X(t))$ are computed from the positions as functions of neighboring positions (see the beginning of the current section) while H_ε^Π is defined in (4.22). Thus, the evolution equation turns into

$$\tfrac{\mathrm{d}}{\mathrm{d}t} x_i(t) = \frac{1}{\varepsilon} \sum_{j=1}^{N} \omega_{ij}(t) \Pi_{ij}(t) \left(x_j(t) - x_i(t)\right), \quad i = 1 \dots N. \tag{5.2}$$

with

$$\omega_{ij}(t) = -\frac{d}{n} \frac{m_j(t) \rho' \left(\dfrac{|x_j(t) - x_i(t)|}{\varepsilon} \right) \dfrac{1}{|x_j(t) - x_i(t)|}}{\displaystyle\sum_{l=1}^{N} m_l(t) \xi \left(\dfrac{|x_l(t) - x_i(t)|}{\varepsilon} \right)}$$

for $i \neq j$ and $\omega_{ii}^k = 0$, where $m_i(t) = m_i(X(t))$ denotes the masses at time t. We observe that $\omega_{ij}(t) \geq 0$ since ρ is nonincreasing in $[0,1]$ and ξ is positive in $]0,1[$. As a first consequence of this rewritten evolution problem we obtain the following comparison result which establishes planar barriers for the flow.

Proposition 5.1 (planar barrier)**.** *Let $(X(t))_{0 \leq t < T}$ be a family of point clouds evolving according to the flow defined in (5.2) up to some time $T \in]0, +\infty]$. Suppose that*

(i) the initial point cloud $X(0) = \{x_i(0)\}_{i=1}^N \subset \mathbb{R}^n$ fulfills $x_i(0) \cdot \nu \leq \mu$ for $i = 1 \dots N$ with $\nu \in \mathbb{R}^n$, $\mu \in \mathbb{R}$,

(ii) for all $0 \leq t < T$, if $x_i(t)$ is a point on the boundary of the convex hull of $X(t)$ then for all points $x_j(t)$ such that $|x_j(t) - x_i(t)| < \varepsilon$, the vector $\Pi_{ij}(t)(x_j(t) - x_i(t))$ at $x_i(t)$ is pointing inside the convex hull of $X(t)$.

Then independently of the choices of masses $m_i(t)$ and for all $0 \leq t < T$,

$$x_i(t) \cdot \nu \leq \mu, \quad \text{for all } i = 1 \dots N.$$

Proof. Assume that the point cloud $X(t)$ is touching the plane $\{x \in \mathbb{R}^n \,|\, x \cdot \nu = \mu\}$ at time $t \geq 0$. Consider any $x_i(t)$ with $x_i(t) \cdot \nu = \mu$. Then, our assumption ensures that $\frac{\mathrm{d}}{\mathrm{d}t} x_i(t) \cdot \nu \leq 0$ and $X(t)$ will not penetrate the plane. □

For $\Pi_{ij} = 2\,\mathrm{Id}$ the assumption in the proposition is obviously fulfilled and for one of the choices $\Pi_{ij} \in \{-2\Pi_{P_j^\perp}, -2\Pi_{P_i^\perp} \circ \Pi_{P_j^\perp}, 2\Pi_{P_j^\perp}\}$ this assumption appears to be a useful constraint to define $\{P_i\}_{i=1,\dots N}$. For $\Pi_{ij} \in \{\Pi_{P_j}, \Pi_{P_i^\perp} \circ \Pi_{P_j}\}$ the assumption will fail in general for most practical choices of the P_i. In fact, in this case the verification of a planar barrier depends in a subtle way on the weights ω_{ij}.

Next, let us consider a spherical comparison principle. A sphere of radius R^0 around a center point $x \in \mathbb{R}^n$ stay spherical under mean curvature motion with radius $R(t) = \sqrt{(R^0)^2 - 2dt}$ and surfaces inside the initial sphere stay inside the evolving spheres until they become singular, *e.g.* at the extinction time (see ([20], Prop. 3.1 and Rem. 4.10) for a measure theoretic version due to Brakke). In what follows, we will here study a discrete counterpart of this comparison principle in the case of point cloud varifolds.

Proposition 5.2 (sphere comparison principle)**.** *For point cloud $X^0 = \{x_i^0\}_{i=1}^N \subset \mathbb{R}^n$ and $z \in \mathbb{R}^n$ define $R^0 = \max_{i=1,\dots,N} |x_i^0 - z|$ and assume that $(X(t))_{0 \leq t < T}$ satisfies (5.1) with $X(0) = X^0$. Then $R(t) = \max_{i=1,\dots,N} |x_i(t) - z|$ fulfills*

$$R(t) \leq \sqrt{(R^0)^2 - 2d \int_0^t c(s) \mathrm{d}s}$$

with

$$c(t) = \min \left\{ \frac{\Pi_{ij}(t)(x_i(t) - x_j(t)) \cdot (x_i(t) - z)}{|x_i(t) - x_j(t)|^2} \,\middle|\, \begin{array}{l} i \in \{1, \dots, N\}, |x_i(t) - z| = R(t) \text{ and} \\ j \in \{1, \dots, N\}, 0 < |x_i(t) - x_j(t)| < \varepsilon \end{array} \right\} \tag{5.3}$$

and $t \leq T$ with T being the extinction time, which is smaller or equal than the supremum over all $t > 0$ for which the argument of the square root is positive.

Proof. Without any restriction assume $z = 0$ and choose any $x_i(t)$ with $R(t) = |x_i(t)|$. Multiplying (5.2) with $x_i(t)$ we obtain

$$\begin{aligned}\tfrac{1}{2}\tfrac{\mathrm{d}}{\mathrm{d}t}|x_i(t)|^2 = \tfrac{\mathrm{d}}{\mathrm{d}t}x_i(t)\cdot x_i(t) &= \frac{1}{\varepsilon}\sum_{j=1}^N \omega_{ij}(t)\Pi_{ij}(t)\,(x_j(t)-x_i(t))\cdot x_i(t)\\ &\le -\frac{c(t)}{\varepsilon}\sum_{j=1}^N \omega_{ij}(t)|x_i(t)-x_j(t)|^2\\ &= \frac{c(t)d}{n}\sum_{j=1}^N \frac{m_j(t)\rho'\left(\dfrac{|x_j(t)-x_i(t)|}{\varepsilon}\right)\dfrac{|x_j(t)-x_i(t)|}{\varepsilon}}{\displaystyle\sum_{l=1}^N m_l(t)\xi\left(\frac{|x_l(t)-x_i(t)|}{\varepsilon}\right)} \le -c(t)d\,,\end{aligned}$$

where we have used $n\xi(s) = -s\rho'(s)$ from (3.1). Thus, we obtain $R(t)^2 \le (R^0)^2 - 2d\int_0^t c(s)\mathrm{d}s$, which proves the claim. □

For $\Pi_{ij} = 2\,\mathrm{Id}$, the constant in (5.7) is $c(t) = 1$ for all t and thus the conclusion of Proposition 5.4 recovers the classical spherical comparison principle $R(t) \le \sqrt{(R^0)^2 - 2dt}$. Indeed, dropping the dependence on time and fixing i and j according to (5.3) and so that $|x_j - z| \le |x_i - z| = R$ we then obtain

$$(x_i - x_j)\cdot(x_i - z) = |x_i - z|^2 - (x_j - z)\cdot(x_i - z) \ge \tfrac{1}{2}|x_i - z|^2 - (x_j - z)\cdot(x_i - z) + \tfrac{1}{2}|x_j - z|^2 = \tfrac{1}{2}|x_i - x_j|^2.$$

Unfortunately, regarding to other choices for Π_{ij}, $c(t)$ strongly depends on the computation of normals and could even be negative.

5.3. Time discrete curvature flow

Let us now proceed with a time discretization of (5.1). It is well–known, for parametric mean curvature flows for instance, that explicit time discretization implies a restrictive stability condition, imposing small time steps. A common solution is then to consider implicit or partially implicit time discretizations. Let us consider a time step $\tau > 0$ and approximate the solution $x_i(t_k)$ at a discrete time $t_k = k\tau$ using the adopted notation

$$\begin{aligned}&m_i^k = m_i(X^k), \quad P_i^k = P_i(X^k), \quad \Pi_{ij}^k = \Pi_{ij}(P_i^k, P_j^k) \text{ as in (4.21)},\\ &X^k = (x_i^k)_{i=1\dots N} \in \mathbb{R}^{nN} \quad \text{and} \quad V^k = \sum_{i=1}^N m_i^k \delta_{(x_i^k, P_i^k)}.\end{aligned}$$

A first natural choice is the implicit scheme (actually implicit with respect to positions X^k but explicit with respect to masses and sets of directions):

$$x_i^{k+1} = x_i^k + \tau H_\varepsilon^\Pi(x_i^{k+1}, \widehat{V^k}) \quad \text{with} \quad \widehat{V^k} = \sum_{i=1}^N m_i^k \delta_{(x_i^{k+1}, P_i^k)}, \tag{5.4}$$

$$V^{k+1} = \sum_{i=1}^N m_i^{k+1}\delta_{(x_i^{k+1}, P_i^{k+1})}, \tag{5.5}$$

where in (5.5) the updated masses m_i^{k+1} and tangent directions P_i^{k+1} are computed from the new positions X^{k+1}. In other words, the positions $X^{k+1} = (x_i^{k+1})_{i=1\dots N} \in \mathbb{R}^{nN}$ must satisfy the following equations for $i = 1\dots N$

$$x_i^{k+1} = x_i^k + \frac{\tau}{\varepsilon}\sum_{j=1}^N \omega_{ij}^{k+1}\Pi_{ij}^k\left(x_j^{k+1} - x_i^{k+1}\right) \tag{5.6}$$

with

$$\omega_{ij}^k = -\frac{d}{n}\frac{m_j^k \rho'\left(\frac{|x_j^k - x_i^k|}{\varepsilon}\right)\frac{1}{|x_j^k - x_i^k|}}{\sum_{l=1}^N m_l^k \xi\left(\frac{|x_l^k - x_i^k|}{\varepsilon}\right)}$$

for $i \neq j$, and $\omega_{ii}^k = 0$. As for the continuous counterpart $\omega_{ij}^k \geq 0$. At first, we obtain as in the time continuous case a comparison principle with planar barriers for the flow.

Proposition 5.3 (planar barrier in the time discrete case)**.** *Suppose that a sequence of point cloud varifolds $(V_k)_k$ is solution of the implicit scheme (5.4). In addition,*

(1) assume that the initial points $X^0 = \{x_i^0\}_{i=1}^N \subset \mathbb{R}^n$ fulfill $x_i^0 \cdot \nu \leq \mu$ for $i = 1 \dots N$ with $\nu \in \mathbb{R}^n$, $\mu \in \mathbb{R}$,

(2) for all k, if x_i^k is a point on the boundary of the convex hull of X^k, then for points x_j^k such that $|x_j^k - x_i^k| < \varepsilon$ assume (implicitly) that $\Pi_{ij}^k(x_j^{k+1} - x_i^{k+1})$ at x_i^{k+1} is pointing inside the convex hull of X^{k+1}.

Then independently of the choices of masses m_i^k

$$x_i^k \cdot \nu \leq \mu, \quad \text{for all } i = 1 \dots N$$

and for all k such that V^k is defined.

Proof. The proof is analogous to the proof of Proposition 5.1 in the time continuous case, now considering $i \in \{1, \dots N\}$ with $x_i^{k+1} \cdot \nu = \max_{j \in \{1,\dots N\}} x_j^{k+1} \cdot \nu$. □

Next, we study a fully discrete version of the sphere comparison property (*cf.* Prop. 5.2).

Proposition 5.4 (time discrete sphere comparison principle)**.** *Suppose that a point cloud $X^0 = \{x_i^0\}_{i=1}^N \subset \mathbb{R}^n$ is contained in a ball B^0 of radius R^0 and centered at z and assume that $(V^k)_k$ is a sequence of point cloud varifolds which are solutions of the implicit scheme (5.4).*
For each $k \geq 1$, define $R^k = \max_{i \in \{1,\dots,N\}} |x_i^k - z|$ and

$$c^k = \min\left\{ \frac{\Pi_{ij}^k(x_i^{k+1} - x_j^{k+1})(x_i^{k+1} - z)}{|x_i^{k+1} - x_j^{k+1}|^2} \,\middle|\, \begin{array}{l} i \in \{1,\dots,N\}, |x_i^{k+1} - z| = R^{k+1} \text{ and} \\ j \in \{1,\dots,N\}, |x_i^{k+1} - x_j^{k+1}| < \varepsilon \end{array} \right\}. \tag{5.7}$$

Then, independently of the choices of masses, for all k such that V^k is defined, the positions $\{x_j^k\}_{j=1}^N \subset \mathbb{R}^n$ are contained in the ball of center z and radius $\sqrt{(R^0)^2 - 2d\tau\sum_{l=1}^k c^k}$.

Let us remark, that in analogy to the time continuous case $c^k = 1$ for $\Pi_{ij} = 2\,\mathrm{Id}$ and hence $\tau\sum_{l=1}^k c^k = t^k$.

Proof. Without loss of generality let $z = 0$. Assume that at time t_k the point cloud X^k satisfies $\max_{j=1\dots N} |x_j^k| \leq R^k$. We choose $i \in \{1, \dots, N\}$ such that $|x_i^{k+1}| = \max_{j \in \{1,\dots N\}} |x_j^{k+1}|$. and proceed in analogy to the proof of Proposition 5.2. Thereby, one obtains

$$|x_i^{k+1}|^2 = x_i^k \cdot x_i^{k+1} + \frac{\tau}{\varepsilon}\sum_{j=1}^N \omega_{ij}^{k+1}\Pi_{ij}^k(x_j^{k+1} - x_i^{k+1}) \cdot x_i^{k+1} \tag{5.8}$$

$$\leq |x_i^k||x_i^{k+1}| - c_k\frac{\tau}{\varepsilon}\sum_{j=1}^N \omega_{ij}^{k+1}|x_j^{k+1} - x_i^{k+1}|^2 \tag{5.9}$$

$$= |x_i^k||x_i^{k+1}| - dc_k\tau \leq \tfrac{1}{2}|x_i^{k+1}|^2 + \tfrac{1}{2}|x_i^k|^2 - dc_k\tau\,.$$

This implies $(R^{k+1})^2 = |x_i^{k+1}|^2 \leq |x_i^k|^2 - 2c_k d\tau \leq (R^k)^2 - 2c_k d\tau$ and thus establishes the claim. □

However, for practical reasons, we rather propose a linearized version of the previous implicit scheme (5.4) in which we choose V^k as the geometric reference in the discrete evolution of the kth time step and we introduce the following semi-implicit scheme

$$x_i^{k+1} = x_i^k + \frac{\tau}{\varepsilon} \sum_{j=1}^{N} \omega_{ij}^k \Pi_{ij}^k \left(x_j^{k+1} - x_i^{k+1} \right) \tag{5.10}$$

which leads to a linear system to be solved in each time step. With $X^k = (x_1^k, \dots, x_N^k) \in \mathbb{R}^{nN}$, we can rewrite this linear system as

$$(M - \frac{\tau}{\varepsilon} L) X^{k+1} = M X^k \tag{5.11}$$

where M is a diagonal matrix of size (nN, nN) defined as

$$M = \begin{pmatrix} \mu_1 \mathrm{I}_n & & \\ & \ddots & \\ & & \mu_N \mathrm{I}_n \end{pmatrix} \quad \text{with} \quad \mu_i = \sum_{l=1}^{N} m_l^k \xi \left(\frac{|x_l^k - x_i^k|}{\varepsilon} \right)$$

and L is a matrix of size (nN, nN), which we can see as a matrix of (N, N) blocks $L_{(i,j)}$ of size (n, n). For a fixed i, the block $L_{(i,j)}$ is the null matrix if $|x_j^k - x_i^k| > \varepsilon$ and

$$L_{(i,j)} = -\frac{d}{n} \frac{m_j^k}{|x_j^k - x_i^k|} \rho' \left(\frac{|x_j^k - x_i^k|}{\varepsilon} \right) \Pi_{ij}^k \quad \text{for } j \neq i \,,$$

$$L_{(i,i)} = -\sum_{j=1, j\neq i}^{N} L_{(i,j)} = \frac{d}{n} \sum_{j=1}^{N} \frac{m_j^k}{|x_j^k - x_i^k|} \rho' \left(\frac{|x_j^k - x_i^k|}{\varepsilon} \right) \Pi_{ij}^k \,.$$

where Π_{ij}^k is the (n, n)–matrix corresponding to the linear operator Π_{ij}^k. The matrix $(M - \frac{\tau}{\varepsilon} L)$ is strongly diagonal dominant and thus an M-matrix. Hence, the system (5.11) is uniquely solvable and one obtains $X^{k+1} = (\mathrm{Id} - \frac{\tau}{\varepsilon} \mathrm{M}^{-1} \mathrm{L})^{-1} \mathrm{X}^{\mathrm{k}}$.

6. Numerical Results

We perform numerical tests with the semi-implicit scheme (5.10). Different from explicit schemes our scheme allows for a time step size of the order of the point sampling distance and turned out to be first order consistent in time. First we test its consistency and robustness to white noise in the simple case of a circle evolving through curvature flow (Sect. 6.1). The absence of singularities allows us to discard most choices for the projector Π_{ij} in (4.21) and we carry on the study with $\Pi_{ij} = 2\Pi_{P_i^\perp}$ in Section 6.2. In particular, we observe that the implicit assumption for the discrete sphere inclusion, though not proven in this case, is satisfied in our numerical experiment (see Fig. 5e). Next we focus in Section 6.3 on curvature flows of curves with crossings and junctions, taking advantage of the flexibility with respect to topological changes of point cloud representation. Our curvature flow is able to converge to both Steiner trees spanning the four vertices of a square in Figure 9. Last, in Section 6.4, we draw our attention to surfaces and recover the minimal cone spanning the edges of a tetrahedron in the limit of our mean curvature flow as well as a candidate minimal surface spanning the edges of a cube, see Figures 10 and 11.

Remark 6.1 (Nearest neighbor graph and *kd*–tree structure)**.** From a practical perspective, we compute neighborhoods thanks to a *kd*–tree structure that is computed with the library *Nanoflann* [4]. Note that the knowledge of the nearest neighbor graph encodes information that can be interpreted as a discrete counterpart to the local

topology of the object. Comparing with triangulated surface, it can be seen as the counterpart to the mesh connectivity information. In fact, in case of triangular surfaces one can either move points and obtain a new mesh with the same connectivity structure, or one can move points and remesh the set of points, which is a computationally demanding operation but often necessary since moving points may create overlaps or crossings in the mesh. In a point cloud, after moving the positions of the points, one has the same choice: one can recompute the nearest neighbor graph or leave it unchanged. As pointed out below, this will be useful to stabilize the point cloud evolution close to triple points. Such operations are straightforward to handle in a *kd*–tree.

6.1. Evolution of circles

As already mentioned when we discussed sphere comparison principle (see Sect. 5.2) a circle of initial radius R_0 evolves into concentric circles of radius $R(t) = \sqrt{R_0^2 - 2t}$ at time t under mean curvature flow. A first step in order to validate our approach is to check this property on our scheme.

We start with a circle of radius $R_0 = 0.5$ uniformly discretized with N points. In Figure 2, we first perform a qualitative comparison of the behavior of the scheme depending on the operator Π_{ij}. In Figures 2e and 2f we observe strong instabilities after short time, while in Figure 2d, instabilities appear after longer time. Consequently, we focus on projection operators tested in Figures 2a, 2b and 2c, that is $\Pi_{ij} \in \left\{\Pi_{P_j}, \Pi_{P_i^\perp} \circ \Pi_{P_j}, \Pi_{P_i^\perp}\right\}$.

As a second step to validate our approach, we then test the robustness with respect to white noise: we introduce an initial white noise of standard deviation s on the circle of radius $R_0 = 0.5$.

In Figure 3a, we observe tangential instabilities with agglomeration of points in very short time. In Figure 3b, we observe that noise is not smoothed but transported, which is reasonable, given that the initial projection onto P_j makes $\Pi_{ij} = \Pi_{P_i^\perp} \circ \Pi_{P_j}$ blind to normal noise. As a consequence of this non-smoothing effect, the speed of evolution is considerably slowed down. In Figures 3c and 3d we observe that noise is smoothed in a few steps. The evolution is then close to the exact one. This is further improved in Figure 3c and in Figure 3d with even higher initial noise. From this first analysis, we conclude that the most robust choice among (4.21) is $\Pi_{ij} = 2\Pi_{P_i^\perp}$ when dealing with discretization of smooth curves.

We then carry on our study with $\Pi_{ij} = 2\Pi_{P_i^\perp}$.

Next, we check the first order convergence in time. To that extend, we compute for the circle evolution the relative mean error after a time T defined as

$$e(T) = \frac{1}{N}\sum_{i=1}^{N} \frac{|R(T) - |x_i(T)||}{R(T)} \quad \text{with} \quad R(T) = \sqrt{R_0^2 - 2T}, \tag{6.1}$$

for successively smaller time steps $\tau = 2^{-k}/N$, $k \in \{0, 1, \ldots, 8\}$. The test is performed on a uniformly discretized circle of radius $R_0 = 0.5$ with $N = 400$ points, the number of points used for the computation of masses is $k_\delta = 3$, of tangent directions is $k_\sigma = 17$ and of curvatures is $k_\varepsilon = 15$. The error $e(T)$ is computed at time $T = 0.1$ while the extinction time is $T_{ext} = R_0^2/2 = 0.125$. In Figure 4, we observe a convergence of first order in time in the case without noise (blue curve labelled "without noise"), while when adding an initial noise independent of τ, the error e_T decay stabilizes and grows (green curve labelled "fixed noise"). So as to understand the behavior of e_T in the case of noise, we perform the same experiment, but adding a white noise of standard deviation $s = \sqrt{2^{-k}}5/N$ which is linked *via* N to the time step size $\tau = 2^{-k}/N$ that is $s^2 = (25/N)\tau$ (red curve labelled "adaptive noise"). We then retrieve the first order convergence in time previously observed without noise. Notice that due to the lack of a Lipschitz bound for the map $t \mapsto R(t)$ near the extinction time $T_{ext} = 0.125$, the error tends to explode for times close to T_{ext} as it is pointed out in Figure 4b.

We eventually study the influence of the number of points k_σ used for the regression and the number of points k_ε used for the computation of the curvature on a circle uniformly discretized with $N = 400$ points. Due to the symmetry of the configuration, all choices happen to be equivalent and we hence add an initial noise of standard deviation $s = 5/N = 0.0125$. The number of points used to compute the mass is 3. We compute the mean error $e(T)$ (6.1) obtained at time $T = 0.1$ for a time step $\tau = 2^{-5}/N = 7.8125\,10^{-5}$. In each box of Figure 4c, the error $e(T)$ corresponding to $(k_\sigma, k_\varepsilon)$ is given.

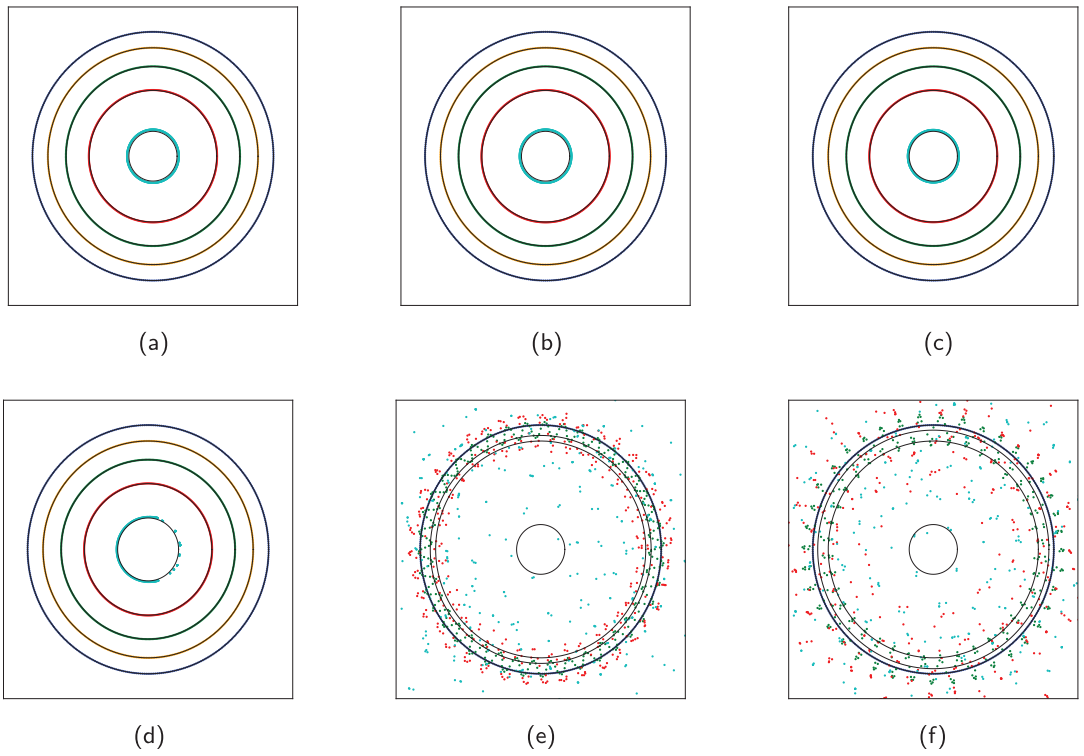

FIGURE 2. Comparison of the results given by the semi-implicit scheme (5.10) for different choices of operator Π_{ij}. The test is performed on a circle uniformly discretized with $N = 400$ points, the number of points for computing the mass is fixed to $k_\delta = 3$, the number of points for the regression is fixed to $k_\sigma = 17$ and the number of points for the computation of curvature is fixed to $k_\varepsilon = 15$, the time step is $\tau = 0.1/N = 0.0005$. The numerical solutions and the exact solutions in black are represented at same times t. Simulations are stopped then resulting in clutter due to noise amplification. (a) $\Pi_{ij} = \Pi_{P_j}$, $t = 0, 0.03, 0.06, 0.09, 0.12$. (b) $\Pi_{ij} = \Pi_{P_i^\perp} \circ \Pi_{P_j}$, $t = 0, 0.03, 0.06, 0.09, 0.12$. (c) $\Pi_{ij} = 2\Pi_{P_i^\perp}$, $t = 0, 0.03, 0.06, 0.09, 0.12$. (d) $\Pi_{ij} = 2\mathrm{Id}$, $t = 0, 0.03, 0.06, 0.09, 0.117$. (e) $\Pi_{ij} = -2\Pi_{P_j^\perp}$, $t = 0, 0.02, 0.03, 0.12$. (f) $\Pi_{ij} = -2\Pi_{P_i^\perp} \circ \Pi_{P_j^\perp}$, $t = 0, 0.01, 0.03, 0.12$.

We observe that the number of points used to compute curvature must be large enough (at least $k_\varepsilon = 13$ in this case) to obtain acceptable errors. The choice of k_σ appears to be less crucial and $k_\sigma = 7$ seems to be already sufficiently large.

6.2. Evolution of more general curves

In this section, we apply our scheme (5.10) with $\Pi_{ij} = \Pi_{P_i^\perp}$ to a point cloud varifold $V = \sum_{i=1}^N m_i \delta_{x_i} \otimes \delta_{P_i}$ associated to the discretization with N points of the following parametrized curve:

$$x(t) = (r(t)\cos t, r(t)\sin t) \quad \text{with} \quad r(t) = \frac{1}{2}\left(1 + r_0 \sin\left(6t + \frac{\pi}{2}\right)\right), \; r_0 = 0, 4 \quad t \in [0, 2\pi[.$$

The parameter interval is uniformly discretized so that for $i \in \{0, \dots, N-1\}$, $x_i = x(2i\pi/N)$, the masses m_i and tangents P_i are then computed from the positions. In Figure 5, we apply our linear semi-implicit scheme (5.10) (for $\Pi_{ij} = 2\Pi_{P_i^\perp}$) to V both with and without noise. The test is performed with $N = 400$ points, the number

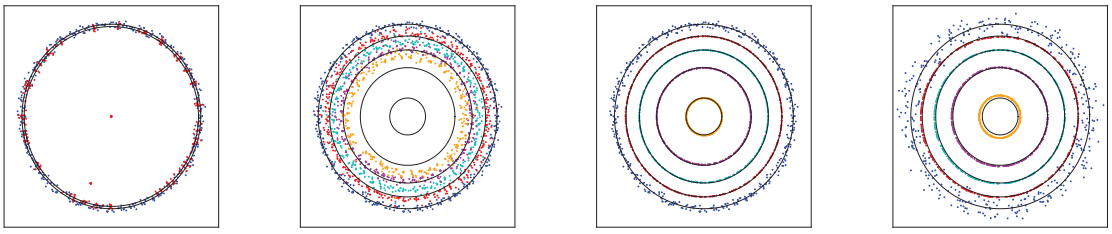

(a) (b) (c) (d)

FIGURE 3. Comparison of the results given by the semi-implicit scheme (5.10) for different choices of operator Π_{ij} when adding white noise. The test is performed on circle uniformly discretized with $N = 400$ points, the number of points for computing the mass is fixed to $k_\delta = 3$, the number of points for the regression is fixed to $k_\sigma = 17$ and the number of points for the computation of curvature is fixed to $k_\varepsilon = 15$, the time step is $\tau = 0.1/N = 0.0005$. The numerical solutions and the exact (black line) solutions are represented at same times t. To the initial circle is added a Gaussian noise with standard deviation $s = 5/N = 0.0125$ in 3a–3c and $s = 15/N = 0.0375$ in 3d. (a) $\Pi_{ij} = \Pi_{P_j}$, $t = 0, 0.006$, $s = 0.0125$. (b) $\Pi_{ij} = \Pi_{P_{i^\perp}} \circ \Pi_{P_j}$, $t = 0, 0.03, 0.06, 0.09, 0.12$, $s = 0.0125$. (c) $\Pi_{ij} = 2\Pi_{P_{i^\perp}}$, $t = 0, 0.03, 0.06, 0.09, 0.12$, $s = 0.0125$. (d) $\Pi_{ij} = 2\Pi_{P_{i^\perp}}$, $t = 0, 0.03, 0.06, 0.09, 0.12$, $s = 0.0375$.

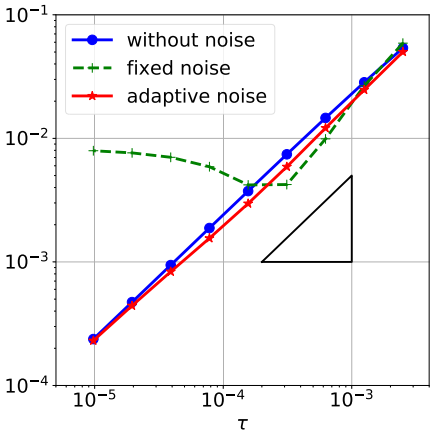

(a)

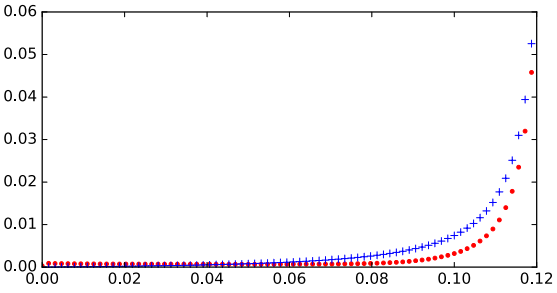

(b)

$k_\sigma \setminus k_\varepsilon$	7	9	13	21	37
7	0.9	0.3	0.03	0.02	0.02
9	0.03	0.1	0.008	0.01	0.009
13	0.05	0.02	0.06	0.01	0.008
21	0.06	0.03	0.01	0.03	0.005
37	0.15	0.08	0.03	0.004	0.01

(c)

FIGURE 4. (a) Decay of the mean error (6.1) at time $T = 0.1$ when the time step $\tau \in \{2^{-k}/N : k = 0, \dots, 8\}$ is refined, $N = 400$. Black triangle indicates slope 1 in log–log scale. (b) Error $e(t)$ represented with respect to time t, for $\tau = 6.2510^{-4}$, in red with initial white noise (of standard deviation 1.2510^{-3}) and in blue without noise. (c) Error $e(0.1)$ for different numbers of points k_σ used for computing tangent and k_ε used for computing curvature.

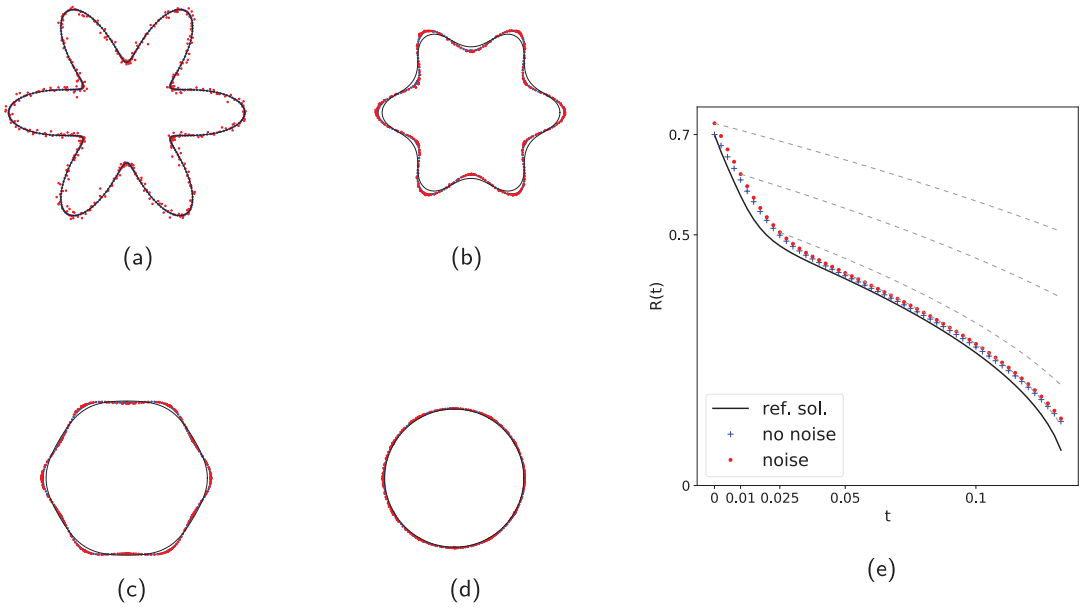

FIGURE 5. *Left figure (a) to (d):* Blue and red point clouds are the results given by our scheme without adding noise for the blue point cloud and with white noise of standard deviation $5/N$ for the red point cloud. The black curve is the reference solution. *Right figure (e):* we compute and represent the minimal radius $R(t)$ of the circle (centered at 0) and including the points at time t, keeping the same parameters and color code as in the left figure. We moreover add grey dashed lines corresponding to the graph of $t \mapsto \sqrt{R(t_0) - 2(t - t_0)}$ for $t_0 \in \{0, 0.01, 0.025, 0.05\}$ and $R(t_0)$ is the radius obtained for the initially noisy shape (red dots). (a) time $t = 0$. (b) time $t = 0.01$. (c) time $t = 0.025$ (d) time $t = 0.05$.

of points for computing the masses is set to $k_\delta = 7$, the number of points for the regression is $k_\sigma = 19$ and the number of points for the computation of curvature is $k_\varepsilon = 25$. We finally choose the time step $\tau = 1/N = 0.0025$. We compare the results to a reference solution computed thanks to a usual parametric mean curvature flow ([19]) with a fine discretization and a time step $\tau_{ref} = 5.10^{-8} = 10^{-5}\tau$. We observe a consistent evolution in Figures 5a–5d, even when some noise is added to the initial shape. In Figure 5e, we check that the discrete sphere inclusion, that was only established for the fully implicit scheme (see Prop. 5.4), is however satisfied in our experiment.

6.3. Singular evolutions in the plane

As we are dealing with point clouds, it is very easy to deal with changes of topologies, especially triple points arising when curves merge are quite naturally captured. Moreover, we know from [10] that the approximate curvature $H^\Pi(x_0, V)$ defined in (3.4) is not only consistent in the smooth context, but as well in presence of singular curvature when $\Pi = \Pi_S$ (*i.e.* $\Pi_{ij} = \Pi_{P_j}$). Even though there is no such rigorous consistency property for $\Pi \in \{\Pi_{(T_{x_0}M)^\perp} \circ \Pi_S, 2\mathrm{Id}, 2\Pi_{(\mathrm{T_{x_0}M})^\perp}\}$ (*i.e.* $\Pi_{ij} \in \{\Pi_{(P_i)^\perp} \circ \Pi_{P_j}, 2\mathrm{Id}, 2\Pi_{(\mathrm{P_i})^\perp}\}$), we compare in Figure 6 the behavior of those operators in the presence of a singularity. More precisely, we consider a junction of three infinite half lines meeting at 0 and we focus on the values of the approximate mean curvature computed in a neighborhood of 0. The lines are uniformly discretized to define a point cloud varifold V with all masses m_i equal and we associate with each point its exact tangent direction P_i : one of the three possible directions (notice

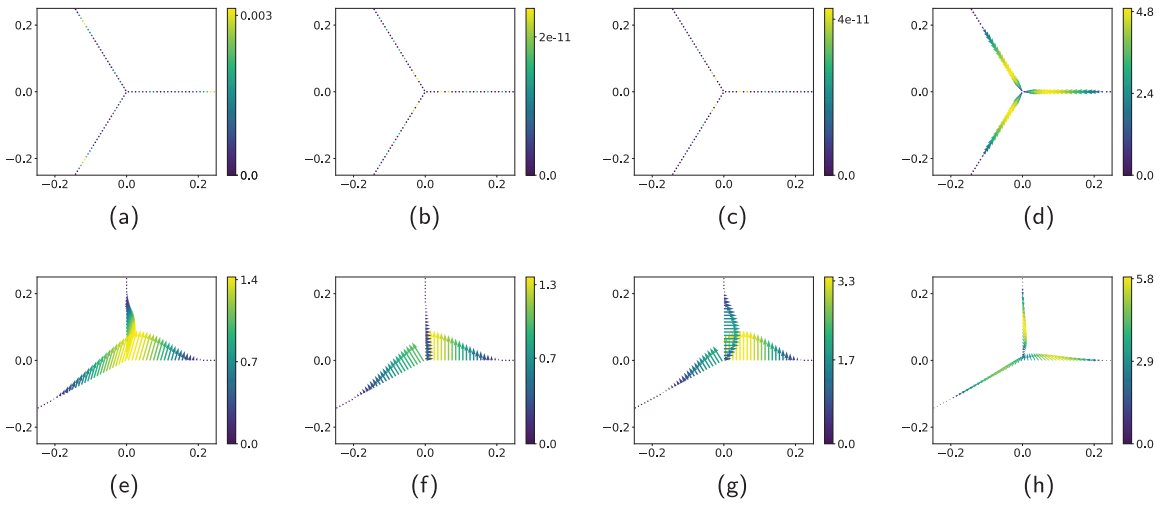

FIGURE 6. Computed mean curvature vector at junction point depending on the chosen projection operator. (a) $\Pi_i j = \Pi_{P_j}$. (b) $\Pi_i j = \Pi_{P_i{}^\perp} \circ \Pi_{P_j}$. (c) $\Pi_i j = 2\Pi_{P_i{}^\perp}$. (d) $\Pi_i j = 2\mathrm{Id}$. (e) $\Pi_i j = \Pi_{P_j}$. (f) $\Pi_i j = \Pi_{P_i{}^\perp} \circ \Pi_{P_j}$. (g) $\Pi_i j = 2\Pi_{P_i{}^\perp}$. (h) $\Pi_i j = 2\mathrm{Id}$.

that there is no point exactly at the junction so that P_i is well–defined). In the computation each neighborhood contains exactly 60 points, corresponding to a disk of radius $\varepsilon \simeq 0.20$ near the singular point 0. We plot the approximate mean curvature vector computed at each point and the norm of this vector is color coded according to the colorbar on the right of each plot while the arrows indicate the direction. Notice that the length of the arrows is rescaled to improve the readability of the plot. The plot is centered at the singularity 0 and the viewing window is scaled such that solely the 60 points closest to the singularity are visualized. In particular the points that are outside do not interfere with the singularity in the computations. We recall that the expected singular curvature of such a junction is $-(u_1+u_2+u_3)\delta_0$ where u_1, u_2, u_3 are the unit vectors pointing in the directions of the half-lines (see Example 2.8).

In Figures 6a–6d, the three half-lines meet with 120 degrees angles, forming a *triple point* having 0 generalized mean curvature (see computations in Example 2.8). We observe that projecting onto the normal $P_i^\perp$ (Figs. 6b and 6c) ensures that the approximate mean curvature is 0 up to a very small error 10^{-11} while the error term (see maximal intensity on the colorbar) is larger 10^{-3} in Figure 6a even in this simple situation. In Figure 6d, there is a tangential component attracting points to the junction point. Furthermore, the arrows are aligned with the lines and point towards 0. In Figures 6e–6h, the three half-lines meet with different angles and we expect some singular curvature to be observed, which can best be seen in Figure 6e.

Unfortunately, choosing $\Pi_{ij} = \Pi_{P_j}$ leads to strong instabilities of the curvature flow as noted previously, see Figure 3 and we carry on with $\Pi_{ij} = 2\Pi_{P_i^\perp}$.

It is then possible to perform mean curvature flow even after the creation of singularities. We propose some examples in $2D$ of such evolutions. In Figure 7, we perform a test on two crossing circles. We observe that both crossing points split up into two triple points almost instantaneously. The different curve segments then merge until they form a single circular curve, which then follows the usual evolution. In this evolution, the circles are discretized with a total of $N = 1000$ points. The number of points used for computing curvature is $k_\varepsilon = 31$, for the tangent is $k_\sigma = 15$ and for the mass is $k_\delta = 7$. The time step is set to $\tau = 1/4N = 2.5 \cdot 10^{-4}$. In Figure 8, we perform a similar test on three crossing circles, which allows to observe several mergers and the formation of multiple triple points. The circles are discretized with a total of $N = 1200$ points. The number of points used for computing curvature is $k_\varepsilon = 31$, for the tangent is $k_\sigma = 15$ and for the mass is $k_\delta = 7$. The time step is set

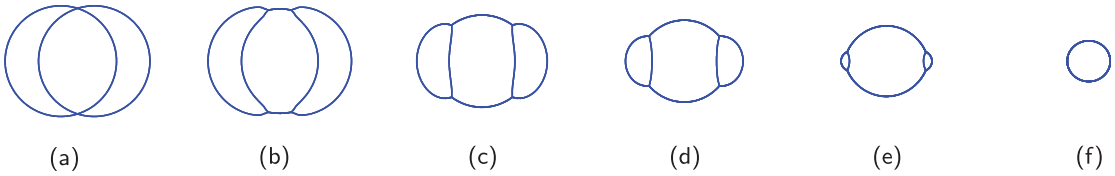

FIGURE 7. Evolution of two crossing circles under discrete curvature flow. (a) time 0. (b) time 0.003. (c) time 0.03. (d) time 0.05. (e) time 0.07. (f) time 0.11.

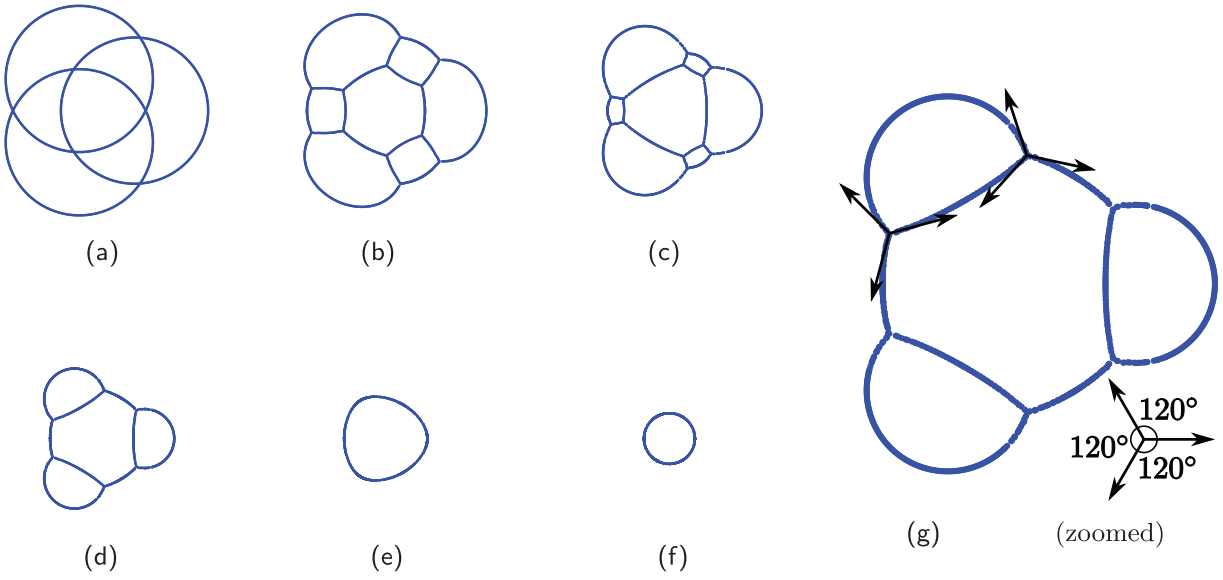

FIGURE 8. Evolution of three circles towards one circle under discrete curvature flow. (a) time 0. (b) time 0.1. (c) time 0.2. (d) time 0.3. (e) time 0.4. (f) time 0.5. (g) time 0.3 (zoomed).

to $\tau = 1/2N \simeq 4.16 \cdot 10^{-4}$. In Figure 8g, a zoom is shown at time 0.3 to provide a better visualization of the triple point configuration.

In Figure 9, we consider an initial configuration consisting of a square whose 4 corners are kept fixed. Evolving this point cloud under curvature flow, we aim at recovering a shortest path connecting the 4 corners, in the limit, usually called Steiner tree. There are 2 shortest paths in this case, because of the symmetry of the configuration of the 4 points, we hence compare our limit configuration to one of the two Steiner trees (plotted in black in each figure) connecting the 4 corners. The experiment is designed as follows, the initial square is discretized with $N = 300$ points.

The number of points used for computing curvature is $k_\varepsilon = 41$ and for computing mass $k_\delta = 7$. The number of points used for computing tangent is $k_\sigma = 11$ in the first evolution (Figs. 9a–9f) and it is $k_\sigma = 15$ in the second evolution (Figs. 9g–9l). The time step is fixed to $\tau = \frac{1}{4N}$. In order to help connectedness to be preserved, we do not recompute the nearest neighbor graph (*i.e.* the *kd*–tree structure, see Rem. 6.1) at each step, but only every 25 iterations. The corners are kept fixed as follows, their positions are included in the linear system (5.11) used to compute positions after a time-step and then, while all other positions are updated, the ones corresponding to the four corners are unchanged.

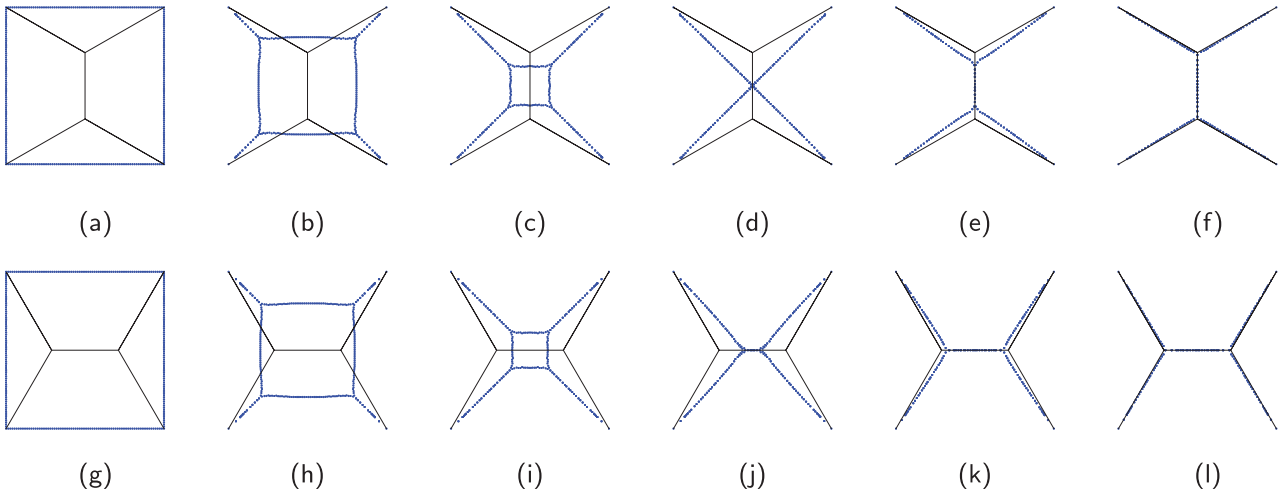

FIGURE 9. Evolution of a square whose corners are fixed to one (a)–(f) or the other (g)–(l) Steiner tree connecting the 4 fixed corners. (a) time 0. (b) time 0.1. (c) time 0.2. (d) time 0.3. (e) time 0.4. (f) time 1. (g) time 0. (h) time 0.1. (i) time 0.2. (j) time 0.3. (k) time 0.4. (l) time 1.

The point cloud is depicted at times 0, 0.1, 0.2, 0.3, 0.4 and 1 as indicated in the legend. The associated Steiner tree is outlined in black and we observe that slight parameter changes may lead to the other Steiner tree. Let us mention here, that specific modulations of the parameters, in particular a too large kernel size for the evaluation of the curvature, eventually leads to a loss of connectedness of the point cloud and thus one ends up with two segments joining two pairs of opposite corners or even worse break up.

6.4. Singular evolutions of surfaces

We now perform numerical tests in $3D$: on a surface leaning on the edges of tetrahedron and on the edges of a cube, and we evidence that, for some parameters, we recover some well–known soap films in the limit of the mean curvature flow. For the tetrahedron, we obtain a cone on the edges which is one of the three possible minimal cones in $\mathbb{R}^3$ (see [37]). For the cube we obtain a surface in Figure 11 (i) with close to planar facets connecting the edges of the cube with a square in the center. This reflects not only experimentally observed soap films but also a theoretical result by Brakke [7] which gives a lower area competitor of the cone over the edges sharing the geometry of our numerical result with slightly bended facets.

It is known that the mean curvature vector points in the direction to choose in order to decrease area. Indeed, the mean curvature vector is the L^2–gradient of the area functional and varifolds generalized mean curvature relies on this characterization. Based on that observation, when the mean curvature flow is well–defined it should yield a minimal surface in the limit. However, when the flow creates singularities it is more complicated to analyze, also on the computational side. For instance, triangulated surfaces are not well–adapted to handle topology changes. Our discrete flow based on point cloud representation allows to observe the evolution from an initial surface spanning the edges of the tetrahedron or the cube to one of the soap films spanning the same boundary. We insist that the discrete flow is automatic, once the parameters are set, there is no further manual intervention. Note that for $2D$ surfaces, creation of holes is an unwanted but successful strategy to decrease area while spanning the same $1D$ boundary (the edges of the tetrahedron here). And in the same line, connecting the edges with many very thin structures rather than a surface gives a lower area since lines have zero area. While in $1D$ we only had to care about wether connectedness was preserved, in $2D$ the topology is richer and the choice of parameters is crucial to discard, when possible, those unwanted behaviors.

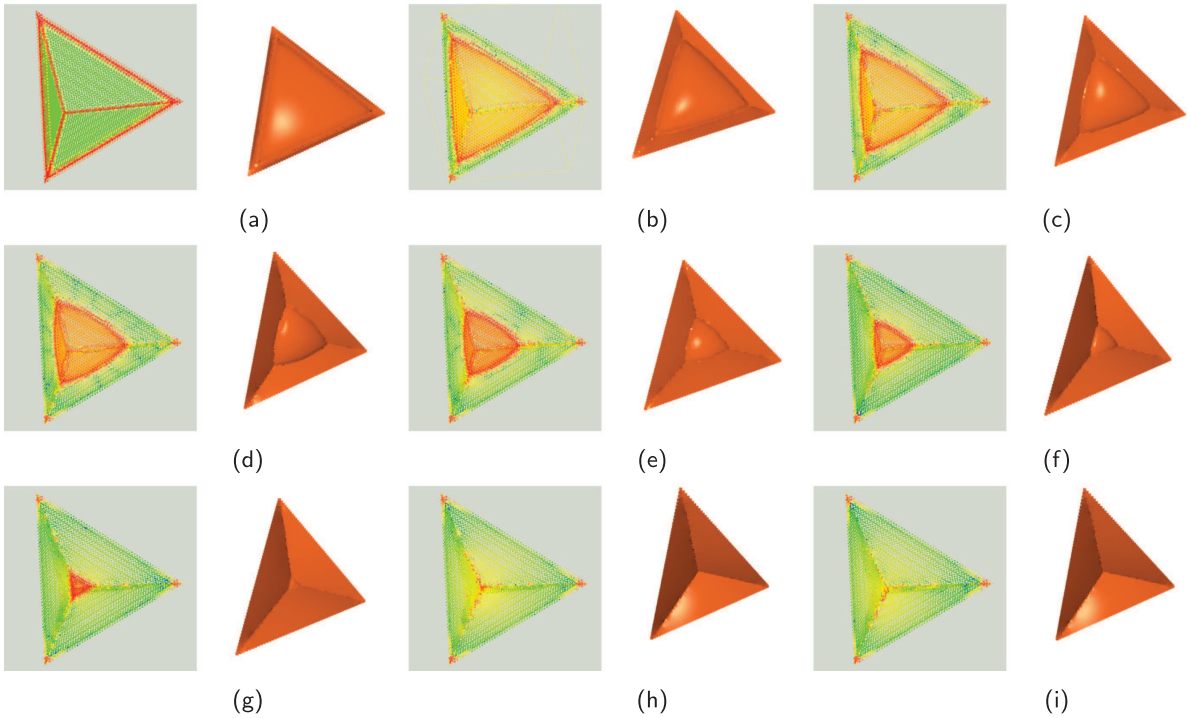

FIGURE 10. Different steps of the semi-linear scheme (5.10) performed on (the surface of) a tetrahedron whose edges are fixed, discretized with $N = 6052$ points and for a time–step $\tau = 0.005$. In explicit one observed an initial detachment of the evolving varifold from the faces of the tetrahedron. These detached pieces then form a bubble collapsing to an interior point of the tetrahedron leaving planar triangular facets with two vertices out of the vertices of the tetrahedron and the third vertex being the interior point. The norm of the approximate mean curvature vector is color coded on the left and on the right a shaded visualization of the point clouds using square shaped splats with proper point normals is shown. (a) Step 1. (b) Step 13. (c) Step 25. (d) Step 37. (e) Step 49. (f) Step 61. (g) Step 73. (h) Step 85. (i) Step 97.

We now give the details of both numerical experiments, starting with the tetrahedron. We begin with a point cloud discretizing the faces of a tetrahedron with $N = 6052$ points. The corners of the tetrahedron 0, $(0, 0, 1)$, $(0, 1, 0)$ and $(0, 0, 1)$ are fixed as well as the edge–points (not moved at iterations). The number of points used for computing curvature is $k_\varepsilon = 26$, tangent is $k_\sigma = 23$ and mass is $k_\delta = 17$. In order to help topology to be preserved, we do not recompute the kd–tree structure at each step, but only every 2 iterations. The time step is fixed to $\tau = 0.005$. The point cloud is depicted every 12 steps of the evolution as indicated in the legend of Figure 10. Edge points are fixed as follows (and similarly to the way corners are fixed for the square in Figure 9): all points including edge points are involved in the semi-implicit computation (5.11) but positions of edge points are never updated. In the last experiment, edge points of the cube are fixed in the same fashion.

We proceed similarly for the cube. The faces of a cube with side–length 1 are discretized with a total of $N = 18600$ points. The number of points used for the computation of curvature is $k_\varepsilon = 21$, tangent is $k_\sigma = 23$ and mass is $k_\delta = 9$.

We do not recompute the kd–tree structure at each step, but only every 50 iterations. The time step is fixed to $\tau = 0.01$. The point cloud is depicted every 400 steps of the evolution as indicated in the legend of Figure 11.

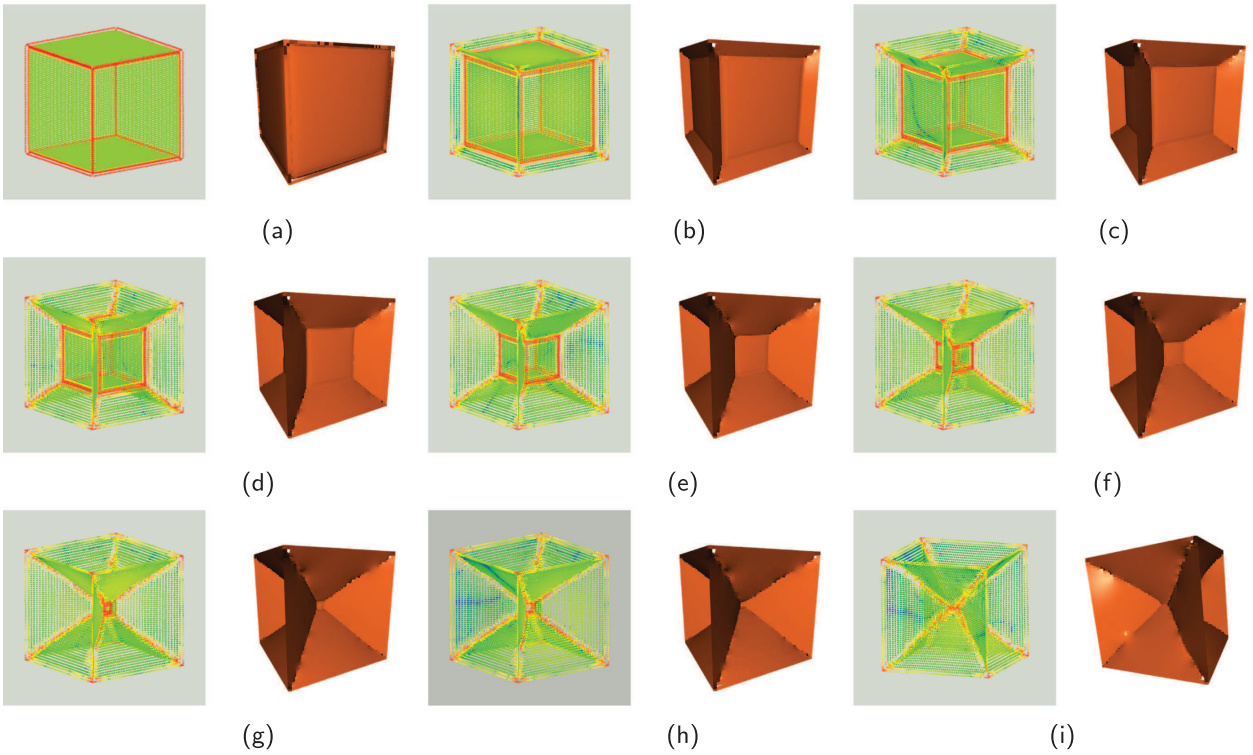

FIGURE 11. Different steps of the semi-linear scheme (5.10) performed on (the surface of) a cube whose edges are fixed, discretized with $N = 18600$ points and for a time–step $\tau = 0.01$. Again, the norm of the approximate mean curvature vector is color coded on the left and on the right a shaded visualization of the point clouds using square shaped splats with proper point normals is shown. (a) Step 1. (b) Step 401. (c) Step 801. (d) Step 1201. (e) Step 1601. (f) Step 2001. (g) Step 2401. (h) Step 2701. (i) Step 2701 rotated.

Acknowledgements. Blanche Buet acknowledges support of CNRS project JCJC 2018 PEPS of INSMI 'A unified framework for surface approximation through varifolds'. Martin Rumpf acknowledges support of the Collaborative Research Center 1060 funded by the Deutsche Forschungsgemeinschaft (DFG, German Research Foundation) and the Hausdorff Center for Mathematics, funded by the DFG under Germany's Excellence Strategy - GZ 2047/1, Project-ID 3906 85813.

REFERENCES

[1] L. Ambrosio, N. Fusco and D. Pallara, Functions of Bounded Variation and Free Discontinuity Problems. Oxford mathematical monographs, Clarendon Press, Oxford, New York (2000).
[2] W.K. Allard, On the first variation of a varifold. *Ann. Math.* (1972) 417–491.
[3] J.W. Barrett, H. Garcke and R. Nürnberg, Parametric approximation of Willmore flow and related geometric evolution equations. *SIAM J. Sci. Comput.* **31** (2008) 225–253.
[4] J.L. Blanco and P.K. Rai, Nanoflann: A C++ header-only library for nearest neighbor search wih KD-trees (2014).
[5] V.I. Bogachev, Measure Theory II. Springer Berlin Heidelberg (2007).
[6] K.A. Brakke, The Motion of a Surface by its Mean Curvature. Mathematical notes (20), Princeton University Press (1978).

[7] K. Brakke, Minimal cones on hypercubes. *J. Geom. Anal.* **1** (1991) 329–338.
[8] K. Brakke, The surface evolver. *Exp. Math.* **1** (1992) 141–165.
[9] E. Bretin and V. Perrier, Phase field method for mean curvature flow with boundary constraints. *ESAIM: M2AN* **46** (2012) 1509–1526.
[10] B. Buet, G.P. Leonardi and S. Masnou, A Varifold Approach to Surface Approximation. *Arch. Ration. Mech. Anal.* (2017).
[11] N. Charon and A. Trouvé, The varifold representation of nonoriented shapes for diffeomorphic registration. *SIAM J. Imaging Sci.* **6** (2013) 2547–2580.
[12] N. Charon, B. Charlier, J. Glaunès, P. Gori and P. Roussillon, Fidelity metrics between curves and surfaces: currents, varifolds, and normal cycles, In Riemannian Geometric Statistics in Medical Image Analysis, edited by X. Pennec, S. Sommer and T. Fletcher. Academic Press (2020) 441–477.
[13] F. Chazal, D. Cohen-Steiner, A. Lieutier and B. Thibert, Stability of curvature measures. *Eur. Symp. Geom. Process.* **28** (2009) 01.
[14] Y.G. Chen, Y. Giga and S. Goto, Uniqueness and existence of viscosity solutions of generalized mean curvature flow equations. *J. Differ. Geom.* **33** (1991) 749–786.
[15] U. Clarenz, M. Rumpf and A. Telea, Finite elements on point based surfaces. In Eurographics Symposium of Point Based Graphics (2004).
[16] D. Cohen-Steiner and J.-M. Morvan, Second fundamental measure of geometric sets and local approximation of curvatures. *J. Differ. Geom.* **74** (2006) 363–394.
[17] K. Deckelnick, G. Dziuk and C.M. Elliott, Computation of geometric partial differential equations and mean curvature flow. *Acta Numer.* **14** (2005) 139–232.
[18] M. Desbrun, M. Meyer, P. Schröder and A. Barr, Implicit fairing of irregular meshes using diffusion and curvature flow. In Proc. of SIGGRAPH 99, Annual Conference Series (1999) 317–324.
[19] G. Dziuk, An algorithm for evolutionary surfaces. *Numer. Math.* **58** (1991) 603–612.
[20] K. Ecker, Regularity Theory for Mean Curvature Flow, Vol. 57. Birkhäuser Basel (2004) 01.
[21] L.C. Evans and J. Spruck, Motion of level sets by mean curvature i. *J. Differ. Geom.* **33** (1991) 635–681.
[22] L.C. Evans and J. Spruck, Motion of level sets by mean curvature iv. *J. Geom. Anal* **5** (1995) 77–114.
[23] L.C. Evans, H.M. Soner and P.E. Souganidis, Phase transitions and generalized motion by mean curvature. *Comm. Pure Appl. Math.* **45** (2006) 1097–1123.
[24] X. Feng and A. Prohl, Numerical analysis of the allen-cahn equation and approximation for mean curvature flows. *Numer. Math.* **94** (2003) 33–65.
[25] T. Ilmanen, Convergence of the allen-cahn equation to brakke's motion by mean curvature. *J. Differ. Geom.* **38** (1993) 417–461.
[26] T. Ilmanen, A. Neves and F. Schulze, On short time existence for the planar network flow. *J. Differ. Geom.* **111** (2019) 39–89.
[27] I. Kaltenmark, B. Charlier and N. Charon, A general framework for curve and surface comparison and registration with oriented varifolds. In 2017 IEEE Conference on Computer Vision and Pattern Recognition (CVPR) (2017) 4580–4589.
[28] L. Kim and Y. Tonegawa, On the mean curvature flow of grain boundaries. *Ann. Inst. Fourier* **67** (2017) 43–142.
[29] C. Mantegazza, M. Novaga and V.M. Tortorelli, Motion by curvature of planar networks. *Ann. Sc. norm. super. Pisa - Cl. sci.* **3** (2004) 235–324.
[30] B. Merriman, J.K. Bence and S.J. Osher, Motion of multiple junctions: A level set approach. *J. Comput. Phys.* **112** (1994) 334–363.
[31] Q. Mérigot, M. Ovsjanikov and L.J. Guibas, Voronoi-Based Curvature and Feature Estimation from Point Clouds. *IEEE Trans. Vis. Comput. Graph.* **17** (2011) 743–756.
[32] U. Pinkall and K. Polthier, Computing discrete minimal surfaces and their conjugates. *Exp. Math.* **2** (1993) 15–36.
[33] H. Schumacher and M. Wardetzky, Variational convergence of discrete minimal surfaces. *Numer. Math.* **141** (2019) 173–213.
[34] N. Sharp and K. Crane, A Laplacian for Nonmanifold Triangle Meshes. *Comput. Graph. Forum* **39** (2020).
[35] L. Simon, Lectures on geometric measure theory, In Vol. 3 of Proceedings of the Centre for Mathematical Analysis, Australian National University. Australian National University Centre for Mathematical Analysis, Canberra (1983).
[36] P. Smereka, Semi-implicit level set methods for curvature and surface diffusion motion. *J. Sci. Comput.* **19** (2003) 439–456.
[37] J.E. Taylor, The structure of singularities in soap-bubble-like and soap-film-like minimal surfaces. *Ann. Math.* **103** (1976) 489–539.
[38] P. Yang and X. Qian, Direct computing of surface curvatures for point-set surfaces. 01 (2007) 29–36.

[39] Y.-L. Yang, Y.-K. Lai, S.-M. Hu and H. Pottmann, Robust Principal Curvatures on Multiple Scales, In Symposium on Geometry Processing, edited by A. Sheffer and K. Polthier, The Eurographics Association (2006).